



Archean granitoid magmatism in the Canaã dos Carajás area: Implications for crustal evolution of the Carajás province, Amazonian craton, Brazil

G.R.L. Feio^{a,b,*}, R. Dall'Agnol^{a,b,c}, E.L. Dantas^d, M.J.B. Macambira^{b,e}, J.O.S. Santos^f, F.J. Althoff^{a,g}, J.E.B. Soares^a

^a Grupo de Pesquisa Petrologia de Granitóides, Instituto de Geociências (IG), Universidade Federal do Pará (UFPA), Rua Augusto Corrêa, 01, Belém, PA, CEP 66075-110, Brazil

^b Programa de Pós-graduação em Geologia e Geoquímica, IG–UFPA, Brazil

^c Instituto Tecnológico Vale, Brazil

^d Laboratório de Estudos Geocronológicos, Geodinâmicos e Ambientais, Universidade de Brasília, Brasília, DF, CEP 70910-900, Brazil

^e Laboratório de Geologia Isotópica, IG–UFPA, Brazil

^f Centre for Exploration Targeting, University of Western Australia, Crawley 6009, Western Australia, Australia

^g Departamento de Geociências, Centro de Filosofia e Ciências Humanas, Universidade Federal de Santa Catarina, Campus Universitário Reitor João David Ferreira Lima, CEP 88040-970, Brazil

ARTICLE INFO

Article history:

Received 7 July 2011

Received in revised form 9 April 2012

Accepted 16 April 2012

Available online 23 April 2012

Keywords:

Geochronology

Nd isotopes

Geochemistry

Archean Granitoids

Crustal evolution

Carajás province

ABSTRACT

Geological mapping, geochemical, and geochronological studies undertaken in the Archean granitoids of the Canaã area in the Carajás province, Amazonian craton, Brazil, led to the identification of new granitoid units. Two compositional groups of granitoids were recognized: (1) minor tonalitic–trondhjemitic units which are both geochemically different (Campina Verde and Pedra Branca) or similar to Archean TTGs (Rio Verde) and (2) major granitic units encompassing calc-alkaline (Canaã dos Carajás, Bom Jesus, and Serra Dourada), transitional (Cruzadão) and alkaline (Planalto) granites. These granitoids form four age groups from Mesoarchean to Neoproterozoic. (1) The protolith of the Pium complex, the Bacaba tonalite and other coeval rocks, as indicated by the presence of inherited zircons, were formed at 3.05–3.0 Ga; (2) at 2.96–2.93 Ga, the Canaã dos Carajás granite and the older rocks of the Rio Verde trondhjemitic were crystallized; (3) at 2.87–2.83 Ga, the Campina Verde tonalitic complex, the Rio Verde trondhjemitic, and the Cruzadão, Bom Jesus and Serra Dourada granites were formed; (4) in the Neoproterozoic, at 2.75–2.73 Ga, the Planalto and Pedra Branca suites and charnockite rocks were crystallized. The granitic units cover more than 60% of the Canaã surface. The Canaã area differs from the Rio Maria and other granite–greenstone terranes by the scarcity of TTGs, dominance of granites, and absence of sanukitoids. The evolution of the Canaã area started at least at 3.2 Ga and was different from that of the juvenile Rio Maria terrane (2.98–2.86 Ga), because of indicating a contribution from pre-existing crust. The Mesoarchean Canaã crust was strongly reworked during the Neoproterozoic (2.75–2.70 Ga) and was probably the substratum of the Neoproterozoic Carajás basin. The evolution of the Carajás province differs from those of Dharwar and Karelian cratons. It approaches the evolution described in the Limpopo belt, in the sense that the Neoproterozoic granitoid magmatism was generated in hot zones of the deep crust, possibly due to collisional tectonic processes.

© 2012 Elsevier B.V. All rights reserved.

1. Introduction

The Carajás province, the largest and best preserved Archean segment of the Amazonian craton (Fig. 1a), northern Brazil, comprises the Rio Maria (RMD) and Carajás domains (Dall'Agnol et al., 2006; Vasquez et al., 2008). The granitoid magmatism and evolution of the RMD have been more extensively studied (Macambira

and Lafon, 1995; Macambira and Lancelot, 1996; Althoff et al., 2000; Souza et al., 2001; Leite et al., 2004; Oliveira et al., 2009a, 2010a; Almeida et al., 2010, 2011) than that of the Carajás domain, where two distinct sub-domains were distinguished: To the north, the Carajás basin formed essentially by Neoproterozoic supracrustal units (Gibbs et al., 1986; Machado et al., 1991; Teixeira and Eggler, 1994; Nogueira et al., 1995; Dall'Agnol et al., 2006) and, to the south, a terrane dominated by Archean granitoids with subordinate granulitic and charnockitic rocks (Vasquez et al., 2008; Oliveira et al., 2010b). This southern terrane is informally known as the 'Transition' sub-domain, interpreted as a probable Mesoarchean substratum, similar to the RMD that was intensely affected by the magmatic and tectonic Neoproterozoic events recorded in the

* Corresponding author at: Grupo de Pesquisa Petrologia de Granitóides, Instituto de Geociências (IG), Universidade Federal do Pará (UFPA), Rua Augusto Corrêa, 01, Belém, PA, CEP 66075-110, Brazil.

E-mail address: gilmara@ufpa.br (G.R.L. Feio).

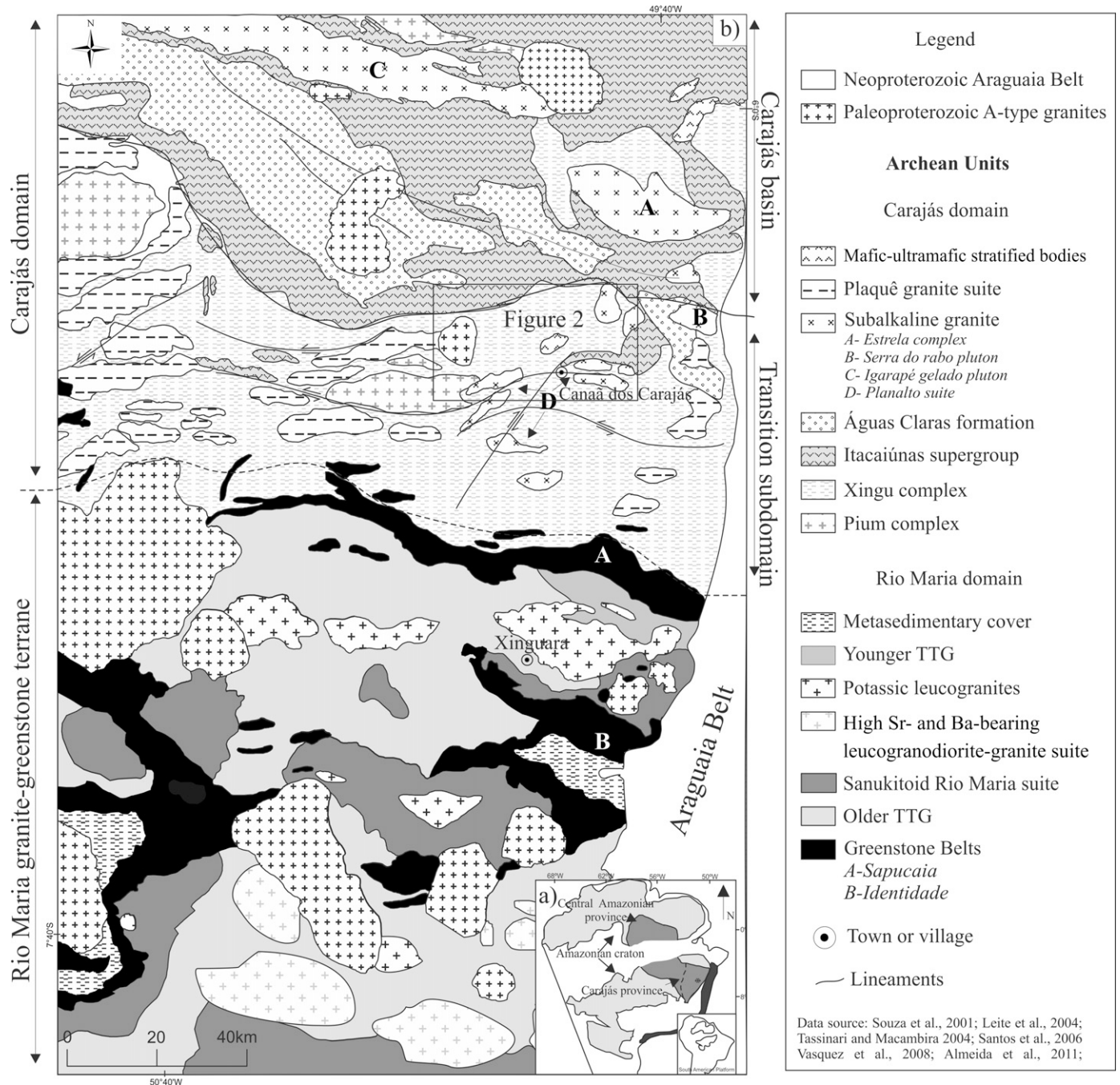


Fig. 1. Simplified geological map of the Carajás province (Leite et al., 2004; Vasquez et al., 2008; Almeida et al., 2011). The dashed line is the proposed boundary between the Carajás domain and the Rio Maria domain; the continuous line divides the Carajás domain in Carajás basin and 'Transition' subdomain (Dall'Agnol et al., 2006).

Carajás basin (Dall'Agnol et al., 2006 and references therein; Domingos, 2009).

The absence of systematic geochemical, geochronological and isotope studies on the Archean granitoid magmatism of the Carajás domain, reflected in the undefined ages and geochemical signature of the major granitoid units exposed in that area, does not allow to constrain models for the crustal evolution of the Carajás domain and, consequently, of the Carajás province.

This paper reports the results of an integrated geochemical, geochronological and Nd isotope study on granitoids of the Canaã dos Carajás region, located in the border between the Carajás basin and the 'Transition' sub-domain. The obtained data are employed to clarify the crustal evolution of the Carajás domain and its

tectonic relationships with the Rio Maria domain. A preliminary geochemical characterization of the different granitoids, in order to distinguish their magmatic series and to establish a comparison between them, is also done. Additionally, this work contributes to the knowledge of the Mesoarchean to Neoproterozoic transition in Archean cratons.

2. Tectonic setting and regional geology of the Carajás province

The Carajás province is located in the southeastern part of the Amazonian craton (Fig. 1a, Machado et al., 1991; Santos et al., 2000;

Tassinari and Macambira, 2004; Dall'Agnol et al., 2006) and their two distinct domains are separated by approximately E–W shear zones (Fig. 1b; Vasquez et al., 2008): To the south, it is exposed the Mesoarchean Rio Maria domain (RMD; 3.0–2.86 Ga; Macambira and Lafon, 1995; Althoff et al., 2000; Souza et al., 2001; Almeida et al., 2011) and, to the north, is the Carajás domain (3.0–2.55 Ga; Gibbs et al., 1986; Machado et al., 1991; Dall'Agnol et al., 2006), which corresponds approximately to the Itacaiúnas shear belt (Costa et al., 1995). The exact limit between the Rio Maria and Carajás domains is still undefined, but it is located approximately to the north of the Sapucaia belt, where there is geophysical evidence suggesting a major tectonic discontinuity (Fig. 1b), separating the more strongly deformed and EW elongated plutonic bodies of the 'Transition' sub-domain from those of the RMD.

The Mesoarchean Rio Maria domain was generated in a period of ~120 Ma and is composed of greenstone belts (3.0–2.90 Ga; Macambira and Lafon, 1995; Souza et al., 2001 and references therein) and several granitoid series: (1) An older TTG series (2.98–2.93 Ga; Macambira and Lancelot, 1996; Althoff et al., 2000; Leite et al., 2004; Almeida et al., 2011); (2) the sanukitoid Rio Maria suite (~2.87 Ga; Macambira and Lancelot, 1996; Oliveira et al., 2009a, 2010a and references therein); (3) a younger TTG series (~2.87–2.86 Ga; Leite et al., 2004; Almeida et al., 2011); (4) a high Sr- and Ba-bearing leucogranodiorite-granite suite (~2.87 Ga; Almeida et al., 2010); and (5) Potassic leucogranites of calc-alkaline affinity (~2.87–2.86 Ga; Leite et al., 1999, 2004).

Compared to the RMD, the Carajás domain (Fig. 1b) presents a more complex evolution. The so-called 'Transition' sub-domain has been poorly studied so far and is formed by strongly deformed Mesoarchean to Neoproterozoic granitoid and gneissic rocks grouped in the Xingu Complex and the northern part of the domain corresponds essentially to the Neoproterozoic Carajás basin.

The Neoproterozoic Carajás basin (Fig. 1b) is formed by banded iron formations, accompanied by a bimodal volcanism metamorphosed in greenschist conditions (Itacaiúnas Supergroup; 2.76–2.74 Ga; Machado et al., 1991; Trendall et al., 1998; Tallarico et al., 2005), and followed by the fluvial to marine siliciclastic deposits of the Águas Claras formation (Nogueira et al., 1995). Several Neoproterozoic subalkaline granite plutons occur in the basin or in adjacent areas (Fig. 1b, 2) and are intrusive into the Itacaiúnas supergroup (~2.76–2.57 Ga; Machado et al., 1991; Barros et al., 2009; Sardinha et al., 2004, 2006; Feio et al., 2012). Near the borders of the Carajás basin (Fig. 1b, 2) several Neoproterozoic mafic-ultramafic layered complexes (Vasquez et al., 2008 and references therein) are also exposed. Sills and dykes of Neoproterozoic hydrothermal-altered gabbros crosscut all these rocks.

The few isotope data available on the Neoproterozoic subalkaline granites of the Estrela Complex (Barros et al., 2009), mafic rocks of the Carajás basin (Gibbs et al., 1986), and Paleoproterozoic A-type granites (Serra dos Carajás suite, Dall'Agnol et al., 2005) indicate that the Carajás basin was formed over a Mesoarchean crustal substratum (~3.0 Ga). It is clear that, differently from the RMD, a large part of the evolution of the Carajás domain was concentrated during the Neoproterozoic when the Carajás basin and subalkaline plutonic magmatism and charnockitic rocks were formed. This implies that the tectonic stabilization of the RMD preceded that of the Carajás domain (Dall'Agnol et al., 2006).

In the Canaã dos Carajás area (Fig. 2; Table 2), located in the border between the Carajás basin and the 'Transition' sub-domain, the oldest rocks exposed were, before the present work, those of the granitic and gneissic Xingu complex (Fig. 1b), the granulites of the Pium Complex (Pidgeon et al., 2000), poorly exposed remnants of Mesoarchean(?) greenstone belts, the Bacaba tonalite (Moreto et al., 2011), and the Canaã dos Carajás potassic leucogranite (Sardinha et al., 2004). The Neoproterozoic (cf. Fig. 2) was marked by the intrusion of the Vermelho mafic-ultramafic layered

complex (Vasquez et al., 2008, and references therein), as well as the trondhjemitic-tonalitic association (Gomes and Dall'Agnol, 2007) designated as Pedra Branca suite in the present work, the Planalto suite granites (Huhn et al., 1999; Sardinha et al., 2004; Feio et al., 2012), Neoproterozoic charnockitic rocks (Gabriel et al., 2010; Feio et al., 2012) and undifferentiated gabbros. To the northern, northeastern and central parts of the mapped area, the Neoproterozoic metavolcanic rocks and banded iron formations of the Itacaiúnas supergroup are exposed. They represent an extension to southeast of the Carajás basin that was affected by the Serra dos Carajás fault and is related to a structure of horsetail splays (Pinheiro and Holdsworth, 1997; Domingos, 2009). Other units exposed in the Canaã area are small plutons of Paleoproterozoic anorogenic granites (Rio Branco and similar granites) and lateritic covers (Fig. 2). Therefore, the areas originally considered to be part of the Xingu complex are in fact formed by different kind of granitoids, and many of them are characterized for the first time in the present work.

3. Geology and petrography

3.1. Mesoarchean Pium granulitic complex

The Pium complex forms a large EW elongated body, disposed parallel to the regional foliation and partially exposed in the southwestern part of the mapped area (Fig. 2). It was described as a Mesoarchean granulitic complex (Pidgeon et al., 2000, and references therein) composed of norite, gabbro, and subordinate quartz-orthopyroxene-bearing rocks, all of them with massive or foliated aspect, generally displaying igneous textures modified by ductile deformation and recrystallization (Ricci and Carvalho, 2006; Santos and Oliveira, 2010). The main geological and petrographic features of the Pium complex and the other units described below are summarized in Table 1.

An enderbite of the Pium complex was dated by SHRIMP U–Pb on zircon and ages of 3002 ± 14 Ma and 2859 ± 9 Ma were obtained, respectively, for the core and rim zones of zircon crystals (Pidgeon et al., 2000). The older age was interpreted as the crystallization age of the protolith of the enderbite and the younger one as the granulite facies metamorphism.

The igneous or metamorphic origin of the Pium complex is now controversial (Vasquez et al., 2008), among other things, because Neoproterozoic orthopyroxene-bearing igneous rocks have been recently identified associated with it (2754 ± 1 Ma, Pb-evaporation on zircon, Gabriel et al., 2010; 2735 ± 5 Ma, LA-MC-ICPMS on zircon, Feio et al., 2012). This indicates the existence of a generation of charnockitic rocks that is clearly younger than the rocks of the Pium complex studied by Pidgeon et al. (2000) and points to the need for additional studies of this complex.

3.2. Mesoarchean tonalites and trondhjemitites

3.2.1. Bacaba tonalite

The Bacaba tonalite (Table 1) is the country rock of the iron oxide–Cu–Au Bacaba deposit and it is intruded by small stocks of gabbros (Moreto et al., 2011). The extension in the surface of this unit is not clearly defined and we have assumed as a preliminary interpretation that the tonalitic rocks exposed to the west of the Bacaba deposit belong to it (Fig. 2). The hydrothermally altered tonalite sampled in drill cores from the mineralized area gave ages around 3.0 Ga (Moreto et al., 2011; cf. Table 2). That tonalite is a foliated, phaneritic fine-grained rock with hornblende and biotite as main mafic minerals.

Table 1
Summary of the field and petrography aspects of the granitoids of the Canaã area.

Units	Age (Ga)	Field and structural aspects	Petrography				
			QAP classification	Texture aspects	Main mafic minerals	Accessory minerals	Secondary minerals
Pium complex	3.0 – protholith cryst. ^a 2.86 – metamorphism ^a	EW-Foliation from ductile deformation ^b	Quartz-gabbro, norite ^b	Fine grained or fine- to medium grained texture ^b	Pyroxene, hornblende ^b	Zircon, titanite, allanite ^b	Chlorite ^b
Bacaba tonalite ^c	3.0 – crystallization	Magmatic foliation	Tonalite	Foliated, fine-grained, gray, and phaneritic. Fine to medium-grained equigranular texture; strong deformed rocks; prophyroclasts of FK surrounded by a fine-grained matrix; elongated ribbons and recrystallized quartz.	Hornblende, biotite	Zircon	Chlorite, epidote, biotite, magnetite
Rio Verde trondhjemite	2.93 – crystallization 2.86 – crystallization	EW to N banded TTG; Folds with vertical or E dipping axes;	Trondhjemite	Medium to fine grained seriated texture; Quartz occurs as elongated polygonal aggregates; FK augen enveloped by fine grained recrystallized aggregates; Bulbous myrmekite intergrowths.	Biotite	Zircon, allanite, and ilmenite	Albite, chlorite, scapolite, biotite, apatite, epidote, carbonate, magnetite, rutile
Canaã dos Carajás granite (gr.)	2.95–2.93 – crystallization	EW-Deformed and mylonitized gr. SE-dipping inverse fault	Monzogranite	Medium to coarse grained granular or porphyritic texture	Biotite	Zircon, magnetite, titanite ± apatite ± allanite	Muscovite, chlorite
Campina Verde tonalite	2.87–2.85 – crystallization	Crosscut by the Serra Dourada granite Magmatic EW-Foliation, locally NS or NE-SW	Two distinct associations: (1) Biotite tonalite to granodiorite with subordinate diorite and monzogranite; (2) biotite-hornblende tonalite with subordinate granodiorite and monzogranite	Medium to coarse grained granular or porphyritic texture	(1) Biotite; (2) biotite, hornblende	Zircon, apatite, allanite, titanite, and magnetite	Scapolite, albite, biotite, apatite, magnetite, actino- lite ± epidote ± sulfides ± chlorite ± quartz

Table 1 (Continued)

Units	Age (Ga)	Field and structural aspects	Petrography				
			QAP classification	Texture aspects	Main mafic minerals	Accessory minerals	Secondary minerals
Bom Jesus granite		(1) NE-SW to EW banded and foliation with vertical SE- to S-dips; (2) sinistral EW to NE-SW shear zones; (3) isoclinal folds with SE-dipping axes.	Monzogranite to -syenogranite	(1) Fine- to medium- to medium- to coarse-grained seriated to porphyroclastic texture; (2) recrystallized lenticular aggregates of quartz; (3) augen shaped porphyroclasts of FK and plagioclase; (4) plagioclase display deformed curved twin lamellae	Biotite	Allanite, titanite, zircon, magnetite \pm ilmenite \pm apatite	Chlorite, rutile, hematite, epidote, carbonates, scapolite, muscovite
Cruzadão granite	2.86–2.85 – crystallization	Folded banded gneiss	Monzogranite to -syenogranite	(1) Coarse- to medium- to medium- to fine-grained seriated texture; (2) core-mantle microstructures; (3) plagioclase show deformed curved twin; (3) recrystallized quartz; undulant extinction and elongated ribbons quartz;	Biotite	Zircon, allanite, apatite, magnetite	Chlorite, epidote, muscovite \pm carbonates
Serra Dourada granite	2.85–2.83 – crystallization		Monzogranite to -syenogranite	Medium- to coarse-grained or subordinate fine-grained texture; (2) little deformed rocks; (3) not pervasive EW-striking vertical foliation	Biotite	Allanite, zircon \pm magnetite \pm ilmenite	Albite, muscovite, biotite, chlorite, epidote, opaque, titanite, quartz, scapolite, and tourmaline

Table 1 (Continued)

Units	Age (Ga)	Field and structural aspects	Petrography				
			QAP classification	Texture aspects	Main mafic minerals	Accessory minerals	Secondary minerals
Pedra Branca suite	2.75 – crystallization	(1) Magmatic banding with subvertical EW-foliation; (2) high-angle stretching lineation dipping to SE	Tonalite and trondhjemite	Medium- to fine-grained and granoblastic texture.	Biotite and hornblende	Titanite, zircon, allanite, apatite, clinopyroxene	Scapolite
Charnockite rocks	2.73 – crystallization		Hypersthene quartz gabbro	Medium- to coarse-grained granular	Pyroxene, hornblende	Titanite, zircon	Scapolite
Planalto suite	2.73 – crystallization	(1) Penetrative EW- to NNW-subvertical foliation; (2) high angle stretching mineral lineation and C-type shear bands; (3) mylonites; (4) dextral EW to NE–SW shear zones.	Monzogranite to syenogranite	(1) Coarse- or medium-grained equigranular to porphyritic; (2) core-and-mantle microstructures; (3) plagioclase shows deformed twinning; (4) quartz as ribbons; (5) mylonites.	Hornblende and biotite	Zircon, apatite, allanite, ilmenite	Scapolite, carbonate, magnetite ± titanite ± fluorite ± tourmaline

^a Pidgeon et al. (2000).^b Santos and Oliveira (2010).^c Moreto et al. (2011).

Table 2

Representative chemical compositions of the granitoids of the Canaã dos Carajás area.

Sample Petrology	AER-79A BTr	AER-11A BTr	AMR-213 BGrd	AMR-102 BLMzG	ERF-123 BMzG	AE-47 BLSG	ARC-65A BHTon	ERF-7C BMzG	ARC-100 BLSG	ERF-102 BLSG	AER-59 BLMzG	AER-27 LMzG	ARC-109 HBSG	AMR-187B HSG	AMR-121D CpxHTon	AMR-191A Tr
Unidade	Rio Verde Trondhjemite		Canaã dos Carajás granite		Bom Jesus gneiss granite		Campina Verde tonalite		Cruzadao granite		Serra Dourada granite		Planalto suite ^a		Pedra Branca suite	
Geog. coordinates (LAT/LONG)	9290747/ 633472	9290489/ 626932	9278407/ 630800	9273289/ 628938	9287124/ 610557	9279910/ 610115	9292330/ 626105	9296314/ 629055	9283661/ 599242	9282649/ 623426	9191062/ 623281	9292497/ 614346	9275089/ 612681	9278743/ 635270	9279712/ 629261	9274706/ 636247
SiO ₂	72.10	73.87	70.56	72.44	71.83	74.43	63.14	69.03	70.90	74.10	72.35	74.61	71.66	72.91	64.03	77.26
TiO ₂	0.24	0.17	0.31	0.16	0.18	0.15	0.51	0.32	0.22	0.15	0.27	0.08	0.44	0.31	1.39	0.34
Al ₂ O ₃	14.80	15.22	14.74	14.84	14.47	13.79	16.23	14.31	14.25	13.35	14.42	13.50	12.77	11.67	14.29	13.25
FeO _t	1.52	0.75	3.03	1.55	1.39	1.03	4.00	3.34	2.55	1.13	1.93	1.17	3.79	4.32	5.33	0.25
Fe ₂ O _{3t}	1.69	0.83	3.37	1.72	1.55	1.15	4.44	3.71	2.83	1.26	2.15	1.30	4.21	4.80	5.92	0.28
MnO	0.02	0.01	0.01	0.04	0.01	0.01	0.03	0.02	0.03	0.02	0.01	0.01	0.03	0.05	0.07	<0,01
MgO	0.69	0.19	0.77	0.37	0.41	0.23	2.71	1.44	0.48	0.29	0.39	0.25	0.36	0.10	1.58	0.01
CaO	2.71	0.51	1.50	2.02	1.59	1.56	5.11	1.15	0.76	1.03	1.94	0.26	1.71	1.67	6.22	2.39
Na ₂ O	5.21	8.13	4.29	4.54	3.83	3.53	4.92	3.99	3.62	3.54	3.95	3.64	3.25	2.99	4.92	5.19
K ₂ O	1.19	0.27	3.17	3.02	4.51	4.56	1.29	4.00	5.60	4.83	3.32	4.80	4.49	4.44	0.53	0.57
P ₂ O ₅	0.07	0.01	0.08	0.05	0.07	0.06	0.21	0.11	0.12	0.05	0.12	0.04	0.09	0.04	0.40	<0,01
LOI	1.20	0.70	1.0	0.7	1.30	0.40	1.20	1.40	0.80	1.30	1.00	1.40	0.70	0.70	0.50	0.60
Total	98.6	99.1	98.5	99.0	98.3	99.4	98.1	97.7	98.5	98.5	98.7	98.4	98.6	98.5	98.8	99.3
Ba	407.2	95.0	961.0	684.0	1658.1	915.0	510.0	889.0	1531.0	519.5	610.1	911.2	1627.0	1459.0	193.0	102.0
Rb	57.5	8.4	108.7	77.6	140.1	135.2	48.1	121.7	227.5	152.8	172.3	149.4	117.3	102.3	6.2	10.8
Sr	763.6	109.9	202.3	282.4	462.5	194.0	704.5	205.8	343.0	200.0	205.2	60.3	144.8	102.9	299.0	193.0
Zr	94.4	108.4	125.6	89.4	167.4	110.6	151.0	107.9	293.2	146.3	148.6	78.2	487.1	503.6	335.8	429.7
Nb	4.0	2.9	6.9	4.9	5.8	3.2	5.6	5.1	3.7	8.6	15.9	25.3	20.9	21.4	25.0	8.2
Y	2.5	3.1	14.8	6.5	2.9	2.5	9.9	6.1	6.4	16.9	11.1	14.2	47.9	66.4	34.6	11.1
Th	5.9	7.8	9.9	5.3	62.6	2.6	6.4	17.7	67.0	63.4	16.8	25.4	23.8	23.4	15.1	8.8
U	0.5	1.4	2.0	0.7	6.7	1.2	2.6	4.2	3.1	18.1	14.4	14.0	3.6	3.4	2.5	2.7
Ga	18.9	17.1	15.7	18.9	17.9	17.3	20.2	20.1	18.2	16.2	22.3	18.5	18.1	19.5	24.1	11.8
Cu	4.6	36.0	28.4	0.8	2.5	7.0	60.0	18.5	165.5	4.8	135.3	66.5	19.4	9.6	1.9	5.1
Pb	2.9	1.1	3.5	2.8	11.0	2.9	5.9	8.8	18.7	14.1	13.4	3.3	5.7	6.6	2.7	3.0
La	19.30	44.30	32.0	15.3	51.30	23.10	43.20	27.40	125.90	81.70	30.20	24.30	64.40	130.00	9.60	7.90
Ce	37.40	44.00	58.8	29.0	87.80	36.90	78.00	52.20	238.90	172.50	62.10	46.70	130.40	249.70	24.50	16.80
Pr	3.54	5.92	6.55	3.23	7.51	3.71	8.92	4.63	26.23	18.35	6.63	4.85	16.31	26.51	3.61	2.45
Nd	11.50	17.50	23.7	11.8	20.90	12.00	31.60	16.90	81.00	59.80	24.20	17.80	62.50	99.60	17.30	10.10
Sm	1.60	1.55	3.69	1.97	2.00	1.35	4.63	2.60	10.85	9.30	4.10	3.30	10.62	15.73	4.14	1.69
Eu	0.53	0.70	0.91	0.40	0.62	0.69	1.21	0.69	1.40	0.71	0.52	0.75	1.84	2.67	1.21	0.98
Gd	0.75	1.10	2.93	1.45	0.92	0.85	3.14	1.29	5.26	5.38	2.81	3.59	8.93	12.67	4.72	1.53
Tb	0.08	0.12	0.43	0.21	0.10	0.10	0.40	0.16	0.62	0.74	0.39	0.42	1.48	2.08	0.65	0.27
Dy	0.47	0.52	2.35	1.15	0.46	0.41	1.88	1.15	2.35	4.02	2.01	2.02	8.36	11.31	4.26	1.59
Ho	0.08	0.09	0.46	0.20	0.07	0.08	0.32	0.19	0.29	0.59	0.32	0.45	1.64	2.24	0.92	0.33
Er	0.21	0.26	1.36	0.54	0.25	0.19	0.90	0.55	0.70	1.51	1.01	1.42	4.73	6.75	2.69	1.12
Tm	0.05	0.04	0.19	0.07	0.05	0.03	0.13	0.08	0.13	0.20	0.14	0.22	0.74	1.02	0.42	0.19
Yb	0.27	0.25	1.27	0.52	0.24	0.21	0.86	0.52	0.91	1.22	0.94	1.61	4.56	6.62	2.84	1.28
Lu	0.05	0.04	0.20	0.06	0.04	0.03	0.12	0.10	0.13	0.19	0.15	0.24	0.68	0.99	0.47	0.21
K ₂ O/Na ₂ O	0.23	0.03	0.74	0.67	1.18	1.29	0.26	1.00	1.55	1.36	0.84	1.32	1.38	1.48	0.11	0.11
Rb/Sr	0.08	0.08	0.54	0.27	0.30	0.70	0.07	0.59	0.66	0.76	0.84	2.48	0.81	0.99	0.02	0.06
Sr/Y	305.4	35.5	13.7	43.4	159.5	77.6	71.2	33.7	53.6	11.8	18.5	4.2	3.0	1.5	8.6	17.4
La/Yb	71.5	177.2	25.2	29.4	213.8	110.0	50.2	52.7	138.4	67.0	32.1	15.1	14.1	19.6	3.4	6.2
Mg ^a	0.45	0.31	0.31	0.30	0.34	0.28	0.55	0.43	0.25	0.31	0.26	0.28	0.14	0.04	0.35	0.07
FeO _t /(FeO _t + MgO)	0.69	0.80	0.80	0.81	0.77	0.82	0.60	0.70	0.84	0.80	0.83	0.82	0.91	0.98	0.77	0.96
(La/Yb)N	51.3	127.1	18.1	21.1	153.3	78.9	36.0	37.8	99.2	48.0	23.0	10.8	10.1	14.1	2.4	4.4
Eu/Eu*	1.30	1.56	0.82	0.69	1.22	1.84	0.92	1.02	0.50	0.28	0.44	0.76	0.56	0.56	0.83	1.83
A/CNK	1.00	1.04	1.12	1.03	1.03	1.02	0.86	1.10	1.06	1.03	1.06	1.16	0.96	0.91	0.72	0.98

BTr, biotite trondhjemite; BHTon, biotite-hornblende tonalite; CpxHTon, clinopyroxene-hornblende tonalite; Tr, trondhjemite; BLMzG, biotite leucomonzogranite; BLSG, biotite leucosyenogranite; BMzG, biotite monzogranite; LMzG, leucomonzogranite; HBSG, hornblende-biotite syenogranite; HSG, hornblende syenogranite.

^a Feio et al. (2012).

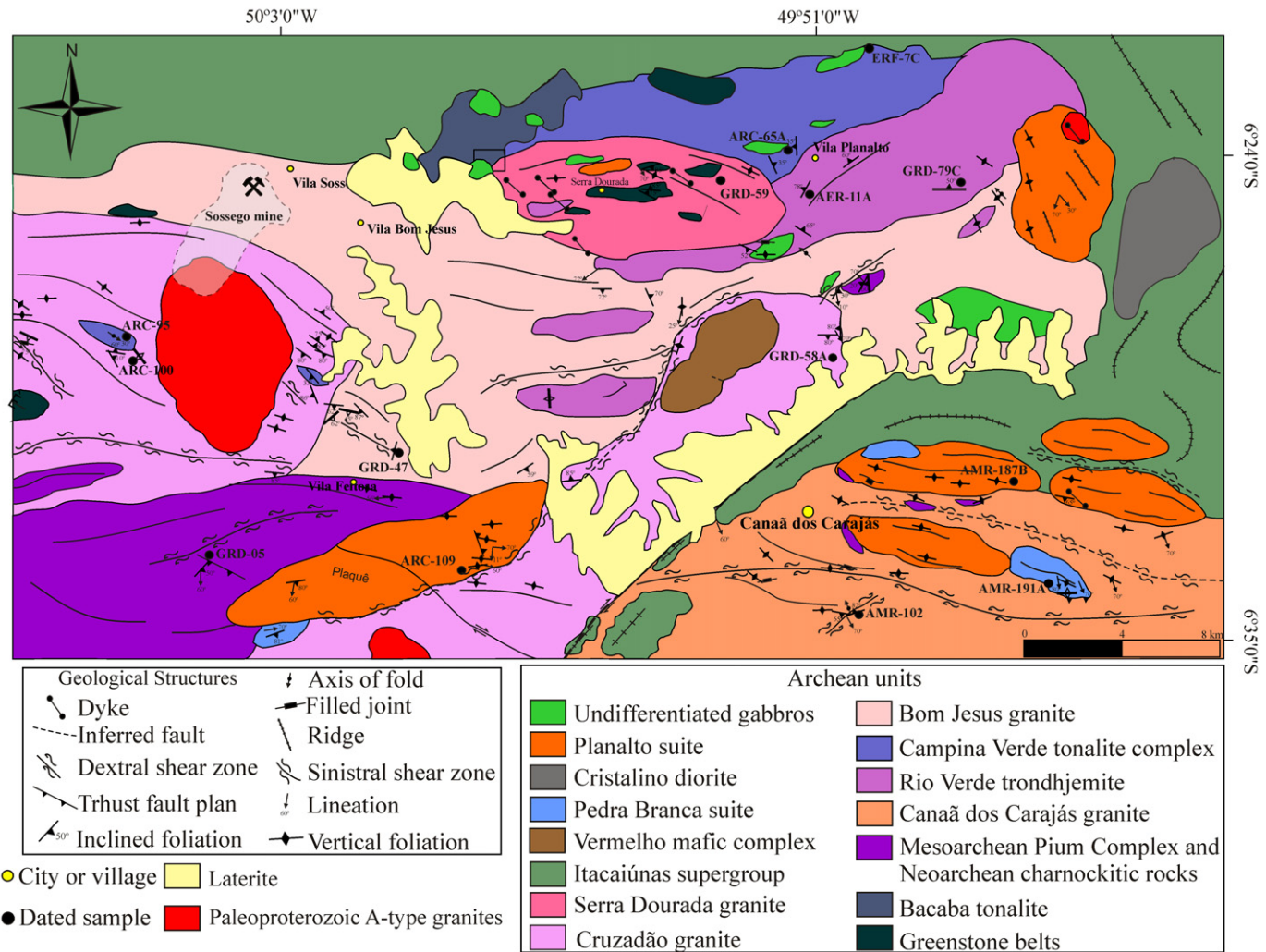


Fig. 2. Geological map of the Canaã area of the Carajás province. Dated samples are indicated by small black circles. The location of this figure is shown in Fig. 1.

3.2.2. Rio Verde trondhjemite

The main exposures of the Rio Verde trondhjemite (Table 1) are located near the Planalto village and extend to the west of the Vermelho intrusion in the center of the Canaã area and to the northeast near the type area of the Planalto granite (Fig. 2). It is in contact with the Bom Jesus granite, Campina Verde tonalitic complex and the Serra Dourada and Planalto granites. The latter gave comparatively younger ages compared to the Rio Verde trondhjemite (see geochronology section). Along the contact with the Serra Dourada granite, the Rio Verde trondhjemite was affected by metasomatism probably related to the intense sodic and subordinate potassic alteration registered in the northern part of the Canaã area (Moreto et al., 2011, and references therein). The dominant trondhjemite varies from texturally homogeneous (Fig. 3b) to banded rocks in which trondhjemitic layers alternate with biotite tonalite.

3.3. Mesoarchean monzogranites and syenogranites

3.3.1. Canaã dos Carajás granite

The Canaã dos Carajás granite occurs in the southeastern part of the study area in the proximities of the Canaã dos Carajás town (Fig. 2; Table 1). It consists of strongly deformed, folded and mylonitized rocks showing penetrative E–W foliation with vertical dip and crosscut by dextral EW or, locally, NE–SW shear zones (Fig. 3a). A SE-dipping inverse fault cut the foliation. Field relationships

between the Canaã dos Carajás granite and other units were not observed, but the inferred western and northern contacts are limited by large shear zones (Fig. 2). Locally, the granite includes metric enclaves of amphibolite.

3.3.2. Campina Verde Tonalitic complex

This complex is exposed near Vila Planalto as an elongated EW-strip in the northern part of the study area (Fig. 2; Table 1). It is in contact to the north with the Itacaiúnas supergroup and to the south with the Rio Verde trondhjemite, Bom Jesus, Serra Dourada and Cruzadão granites. Two distinct associations were distinguished: (1) biotite tonalite to granodiorite (Fig. 3d) with subordinate diorite and monzogranite that dominate in the northern domain of the unit, and (2) biotite-hornblende tonalite with subordinate granodiorite and monzogranite, exposed in the quarry near Vila Planalto (Fig. 3e) and extending to the west in the southern domain of the unit close to the contact with the Serra Dourada granite. The main mineralogical contrast between these associations is related to the modal content of amphibole. Leucogranite veins cut all these rocks.

In addition, hornblende tonalites, similar in mineralogy to those of the southern domain, occur in close association with the Cruzadão granite (Fig. 3f) in the central-western part of the area, near the Rio Branco granite (Fig. 2). The different rock varieties of the tonalitic complex are characterized by a remarkable magmatic



Fig. 3. Field aspects of the granitoids of the Canaã area. (a) Foliated Canaã dos Carajás granite crosscut by dextral shear zones; (b) Regular banding in the Rio Verde trondhjemite; (c) intercalated bands of Bom Jesus granite and trondhjemite correlated with the Rio Verde trondhjemite; (d) detail of the biotite granodiorite facies of the Campina Verde tonalitic complex; (e) the Serra Dourada granite cutting the biotite-hornblende tonalite facies of the Campina Verde tonalitic complex in a quarry near the Planalto village; (f) intercalated bands of Cruzadão granite and Campina Verde tonalite; (g) Isotropic aspect of the Serra Dourada granite; (h) subvertical mineral lineation in a trondhjemite of the Pedra Branca suite; and (i) oval-shaped, deformed K-feldspar megacrysts in the Planalto granite.

~EW-foliation marked by the alignment of crystals of plagioclase and mafic minerals. Locally, the foliation is oriented along NS or NE–SW directions.

3.3.3. Bom Jesus granite

The Bom Jesus granite (Table 1) is exposed in the central-eastern part of the mapped area. It consists essentially of banded and foliated granite oriented along NE–SW to EW with vertical or steep dips to SE and S. Sinistral mylonitic EW to NE–SW shear zones crosscut the granite and apparently control the strike of their major structures. Locally, isoclinal folds with SE-dipping axes were registered. Late coarse or fine-grained granitic veins are associated with the granites. Field aspects suggest that this granite had a complex evolution and this is reinforced by geochronological data (see below).

The Bom Jesus granite and the Rio Verde trondhjemite are disposed in semi parallel NE-oriented strips (Fig. 2) and they show strong interaction along the contacts. In the field, the rocks of both units occur associated and intercalated bands of granite and trondhjemite composition are commonly observed (Fig. 3c). This suggests that both units were submitted to the same event of intense ductile deformation. The Bom Jesus granite contains enclaves of amphibolites and is cut by epidote and quartz-feldspar veins. Except for the contact with the Rio Verde trondhjemite, the relationships between the Bom Jesus granite and the other units were not observed in the field.

3.3.4. Cruzadão granite

The Cruzadão granite (Table 1) shows dominant NW–SE- to EW-striking foliation and was locally affected by NW–SE- to EW shear zones. Two distinct areas of its occurrence were identified. The first one is located in the central-western part of the mapped area, where the granite is in contact to the north with the Campina Verde tonalite and Itacaiúnas supergroup, to the south with the Pium complex and to the east with the Bom Jesus granite (Fig. 2). In this sector, the Cruzadão granite is exposed in small hills and is intruded by the Paleoproterozoic Rio Branco granite. It is also locally associated with hornblende tonalites which are tentatively correlated with the Campina Verde tonalite. Both rocks define strongly banded structures with intercalated bands of granitic and tonalitic composition (Fig. 3f) which were folded, suggesting that these rocks had a coeval emplacement and were submitted to similar ductile deformational processes.

The second large occurrence of the Cruzadão granite defines a NE–SW-oriented strip located in the central-southern part of the area (Fig. 2). To the east, this intrusion has a tectonic contact with the Canaã dos Carajás granite and the Itacaiúnas supergroup, and to the north with the Bom Jesus granite. It is intruded by the Vermelho mafic body, a pluton of the Planalto suite and a small stock of the Pedra Branca suite. The field relationships between different units were not observed in the field and the local stratigraphy was defined on the basis of geochronological data.

3.3.5. Serra Dourada granite

The Serra Dourada granite is a sub-circular stock, located near the Serra Dourada village in the northern part of the Canaã area (Fig. 2; Table 1). Remnants of greenstone belts are involved by the granite. It is intrusive into the Campina Verde tonalitic complex as observed in the northwestern contact between both granitoids and in a quarry immediately to the west of Vila Planalto (Fig. 3e). Conclusive field relationships between it and the Rio Verde trondhjemite and the Bom Jesus granite were not observed. This granite show also a spatial association with abundant small bodies of mafic rocks that apparently cut the granite but their contact relationships are not exposed.

The Serra Dourada granite is composed mainly of medium- to coarse-grained pink-colored rocks (Fig. 3g) which are crosscut by pegmatite and aplitic veins. The major part of the stock is formed by little deformed rocks. A non-pervasive EW-striking vertical foliation is observed locally and mylonitized rocks are found along shear zones.

3.4. Neoproterozoic tonalites and trondhjemites (Pedra Branca suite)

The Pedra Branca suite is composed of sodic granitoids exposed in the southern part of the study area. It occurs as small stocks spatially associated with the Planalto Suite (Fig. 2) but the contact relationships between this unit and the Planalto suite and also with other Archean units are not clearly exposed in the field.

The rocks of the Pedra Branca suite are strongly deformed and commonly show a magmatic banding, with alternation of decimeter- to meter-thick tonalitic and trondhjemitic bands and subvertical EW foliation related to a ductile deformation. A high angle SSE-dipping thrust fault was identified in the stock located in the southeastern part of the mapped area (Fig. 2). It intercepts the primary foliation and is apparently related to the action of a late NS-compressive strain (Gomes and Dall'Agnol, 2007). High-angle stretching lineation dipping to the SE is locally present (Fig. 2, 3h).

3.5. Neoproterozoic granites and charnockites

3.5.1. Planalto suite

The Planalto suite was described in great detail by Feio et al. (2012) and just a synthesis of its main aspects will be given here. It consists of several lenticular granite stocks with less than 10 km in the largest dimension, located in the areas of stronger deformation and oriented concordantly to the dominant EW-trending regional structures or, eventually to NE–SW or NS (Fig. 2). The Neoproterozoic Planalto suite is intrusive into the Mesoarchean granitoid units, into the mafic Pium complex, and into the Neoproterozoic supracrustal Itacaiúnas supergroup (Fig. 2). In general, this suite is associated spatially with the Pium complex and the Pedra Branca suite.

The Planalto granite (Table 1) shows penetrative EW- to NNW-subvertical foliation locally accompanied by a high angle stretching mineral lineation and C-type shear bands. Mylonites are found along sinistral or subordinate dextral EW to NE–SW shear zones.

3.5.2. Charnockite rocks

Neoproterozoic charnockites occur in close association with the Pium complex and cannot be individualized in the scale adopted for the geological mapping. However, outside the study area, relatively large bodies of such rocks were recognized (Gabriel et al., 2010) and there is increasing evidence that they can have an important role in the evolution of the 'Transition' sub-domain. In that sub-domain, these orthopyroxene-bearing rocks have quartz norite to leucoenderbite composition and occur associated with the Pium complex and Planalto suite (Feio et al., 2012). The field relationships between the charnockites and the Planalto granite are complex but apparently some interaction between both magmas has happened suggesting that they coexisted in the partially molten state.

4. Geochemistry

4.1. Introduction

In this section, the geochemical characteristics of the Archean granitoid in the Canaã area are presented, (Table 3) in order to distinguish their magmatic series and to make comparisons between them. Representative chemical analyses of the studied granitoid units are shown in Table 1 and the analytical methods are presented in Appendix A. For the discussion of the

Table 3
Synthesis of geochemical data of the granitoids of the Canaã area.

Units	SiO ₂	Al ₂ O ₃	ACNK	FeO _t /(FeO _t + MgO)	K ₂ O/Na ₂ O	Sr/Y	(La/Yb) _N	Eu/Eu*	Magmatic series
Rio Verde trondhjemitite	69.7–76.2	13.5–15.8	1.0–1.1	0.63–0.89	0.17–0.61	25–305	34–127	0.6–2.0	Low- to medium-K ₂ O calc-alkaline
Campina Verde tonalite to granodiorite	62.9–69.0	13.5–16.4	0.75–1.11	0.5–0.76	0.26–1.20	11–80	9–60	0.7–1.3	Calc-alkaline
Pedra Branca suite	55.7–79.5	12.9–15.1	0.62–1.08	0.71–0.97	0.09–0.19	4–182	1–12	0.4–3.9	Tholeiitic to calc-alkaline
Canaã dos Carajás granite	70.6–72.9	14.3–14.8	1.0–1.1	0.8	0.67–1.05	13–43	7–21	0.7–1.1	Calc-alkaline
Bom Jesus granite	71.8–74.4	13.2–14.8	1.02–1.08	0.77–0.84	0.98–1.60	61–376	86–329	0.5–1.2	Calc-alkaline
Cruzadão granite	70.3–74.3	13.3–14.4	0.98–1.09	0.77–0.85	1.25–1.97	2–53	19–120	0.3–0.5	Calc-alkaline to alkaline
Serra Dourada granite	72.3–75.4	13.5–14.4	1.08–1.16	0.82–0.90	0.89–1.94	4–18	23–63	0.4–0.8	Calc-alkaline
Planalto suite	70.4–75.5	11.4–13.1	0.91–1.09	0.88–0.99	1.24–2.00	1–4	5–17	0.3–0.7	Alkaline

geochemical data, these granitoids will be assembled in two different groups according to the dominant rocks and independent of their ages: (1) tonalite-trondhjemitite and subordinate associated rocks; (2) granitic rocks. The first group encompasses two Mesoarchean units, the Rio Verde trondhjemitite and the Campina Verde tonalitic complex, and the Neoproterozoic Pedra Branca suite. Five granite units have been distinguished in the second group. Four of them are of Mesoarchean age (the Canaã dos Carajás, Bom Jesus, Cruzadão, and Serra Dourada granites) and one was formed during the Neoproterozoic (Planalto suite). The geochemistry and origin of the Neoproterozoic Planalto suite and of the Mesoarchean granites were discussed in more detail by Feio et al. (2012) and Feio and Dall'Agnol (submitted for publication), respectively.

4.2. Geochemical classification

In the normative An–Ab–Or plot (Fig. 4a), rocks of the tonalitic-trondhjemitic units plot mostly in the tonalite and trondhjemitite fields but they occupy distinct areas of the diagram, whereas those of the five granite units plot in the granite field and are partially superposed. The rocks of the first group plot dominantly in the tonalite (trondhjemitite) field with the varieties of the Campina Verde tonalite complex showing more variable composition and the granitic rocks plot in the monzogranite and syenogranite fields with subordinate granodiorite (Fig. 4b, PQ diagram). In the K–Na–Ca plot (Fig. 4c), the Rio Verde trondhjemitite and the Pedra Branca suite samples are concentrated in the field of Archean TTGs but the latter show lower K contents. The Campina Verde tonalitic complex samples are dispersed on the diagram with a clear distinct distribution of the hornblende- or biotite-dominated varieties. All granite units are disposed along the calc-alkaline trend (Fig. 4c), but they can be distinguished by their variable K-contents. The rocks of the Pedra Branca suite are metaluminous and show a large chemical variation, whereas those of the Campina Verde tonalitic complex can be either metaluminous (amphibole-bearing varieties) or peraluminous (biotite-dominated facies) and those of the Rio Verde trondhjemitite are essentially peraluminous rocks. The Mesoarchean granite units are peraluminous, whereas the Neoproterozoic Planalto suite granites that are dominantly metaluminous (Fig. 4d, AB diagram). In the SiO₂ vs. FeO_t/(FeO_t + MgO) diagram (Fig. 4e), the Rio Verde trondhjemitite and the Campina Verde tonalitic complex show the lowest FeO_t/(FeO_t + MgO) and are magnesian granitoids. The Pedra Branca suite has a relatively high FeO_t/(FeO_t + MgO) compared to the other units of the first group and can be classified as a ferroan series (Frost et al., 2001). The Mesoarchean granite units plot in the border between the magnesian and ferroan fields (Fig. 4e) and represent more probably, strongly fractionated

magnesian granites. The Planalto suite granites show the highest values of FeO_t/(FeO_t + MgO) and are typical ferroan granites (Frost et al., 2001). In the 100 * (MgO + FeO + TiO₂)/SiO₂ vs. (Al₂O₃ + CaO)/(FeO + K₂O + Na₂O) diagram, the Mesoarchean granites are all strongly fractionated and vary from calc-alkaline to transitional between calc-alkaline and alkaline (Cruzadão granite). In turn, the Planalto suite granites show a clear alkaline character.

The three tonalitic-trondhjemitic units are clearly distinguished in the TiO₂ vs. SiO₂ diagram (Fig. 5a). The Pedra Branca suite shows characteristics between tholeiitic and calc-alkaline, whereas the Rio Verde trondhjemitite and Campina Verde tonalite define calc-alkaline trends (AFM-diagram in Fig. 5b). The Pedra Branca suite is depleted in K₂O, the Rio Verde trondhjemitite has low- to medium-K₂O contents and the Campina Verde tonalite complex rocks show a strong variation of K₂O (Fig. 5c).

4.3. Trace elements

4.3.1. Tonalitic-trondhjemitic units

The Pedra Branca suite differs from the other units by its higher Zr and lower Rb contents (Fig. 6a, Rb vs. Zr diagram; cf. also Gomes and Dall'Agnol, 2007). The Rb contents of the Campina Verde complex tend to be higher compared to the Rio Verde trondhjemitite. The La/Yb vs. Sr/Y ratios tend to increase from the Pedra Branca suite to the Campina Verde complex and attain the highest values in the Rio Verde trondhjemitite (Fig. 6b). The REE patterns (Fig. 6c) of the three units are also clearly distinct due to the contrast in the degree of fractionation of heavy REE (HREE). Eu anomalies are absent or discrete (positive or negative) in all three units.

The dominantly tonalitic-trondhjemitic units show clear geochemical contrasts that point for their independent origin. The Pedra Branca suite, despite its dominant lithologies, is enriched in TiO₂, Zr, and Y, has no geochemical affinities with the Archean TTG series and must have been originated by different processes or derived from distinct sources than the TTGs (Gomes and Dall'Agnol, 2007). The Campina Verde tonalitic complex also differs from the classical Archean TTG series because it defines an expanded magmatic series that has affinity with calc-alkaline series (Fig. 5b). Besides, its amphibole- and biotite-dominated varieties tend to follow two distinct near vertical trends in the K–Na–Ca plot (Fig. 4c) and are not concentrated exclusively in the field of classical Archean TTGs (Martin, 1994). Only the Rio Verde trondhjemitite has geochemical affinities with TTGs, including those of the Rio Maria domain (Fig. 5b).

4.3.2. Granitic units

In the Zr vs. Rb/Sr plot (Fig. 7a), the Zr-enriched character of the Planalto suite is remarkable, whereas the Mesoarchean

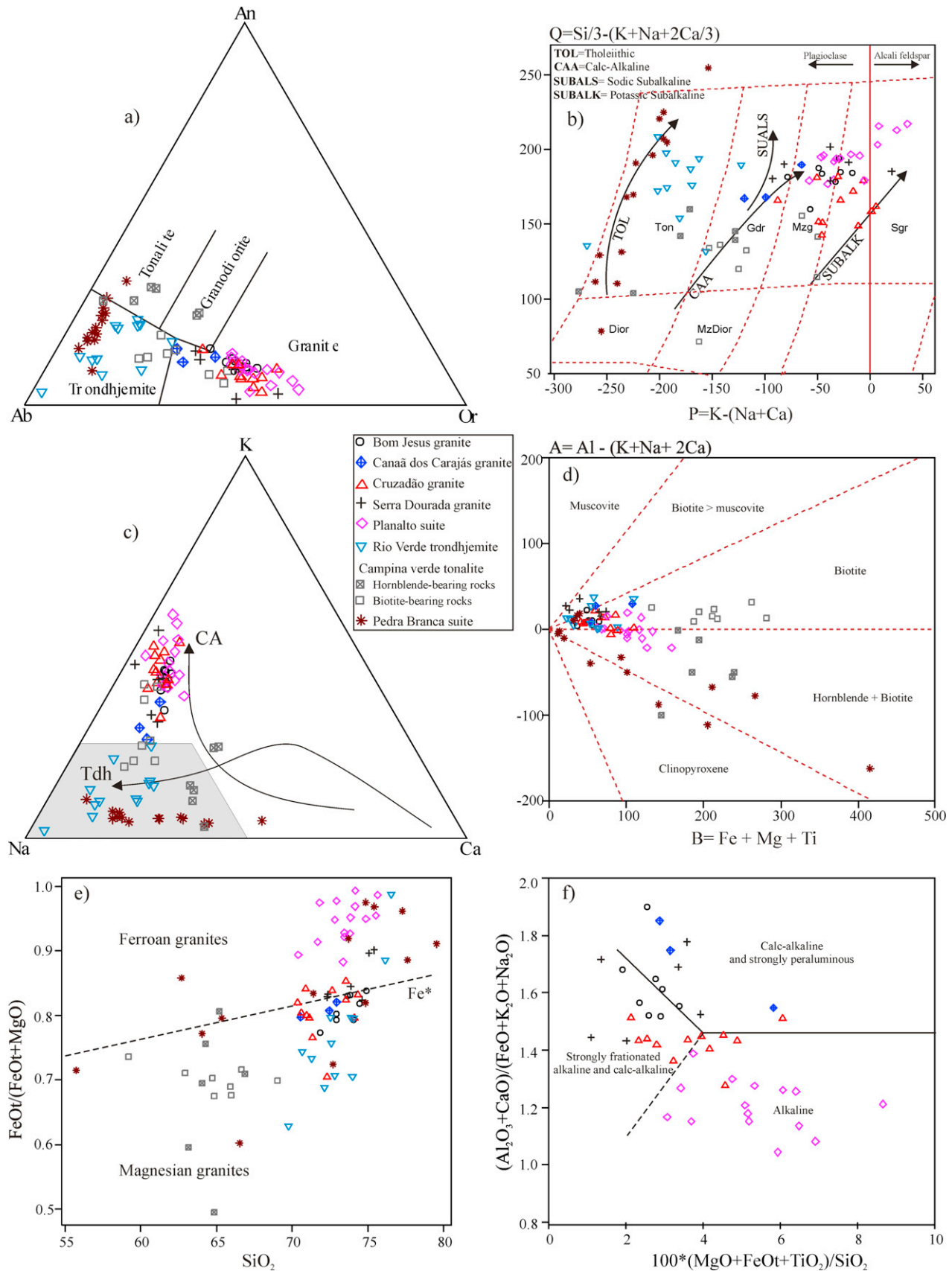


Fig. 4. Geochemical diagrams showing the distribution of the granitoids of the Canaã area. (a) Normative feldspar triangle (O'Connor, 1965) with fields from Barker (1979); (b) P-Q diagram (Debon and Le Fort, 1988); (c) K-Na-Ca plot with trends for calc-alkaline (CA) and trondhjemite (Tdh) series (Barker and Arth, 1976) and gray field of Archean TTG (Martin, 1994); (d) B-A diagram (Debon and Le Fort, 1988); (e) SiO₂ vs. FeO/(FeO+MgO) plot (ferroan and magnesian granites fields of Frost et al. (2001)); and (f) major element discrimination diagram for leucogranites (Sylvester, 1989).

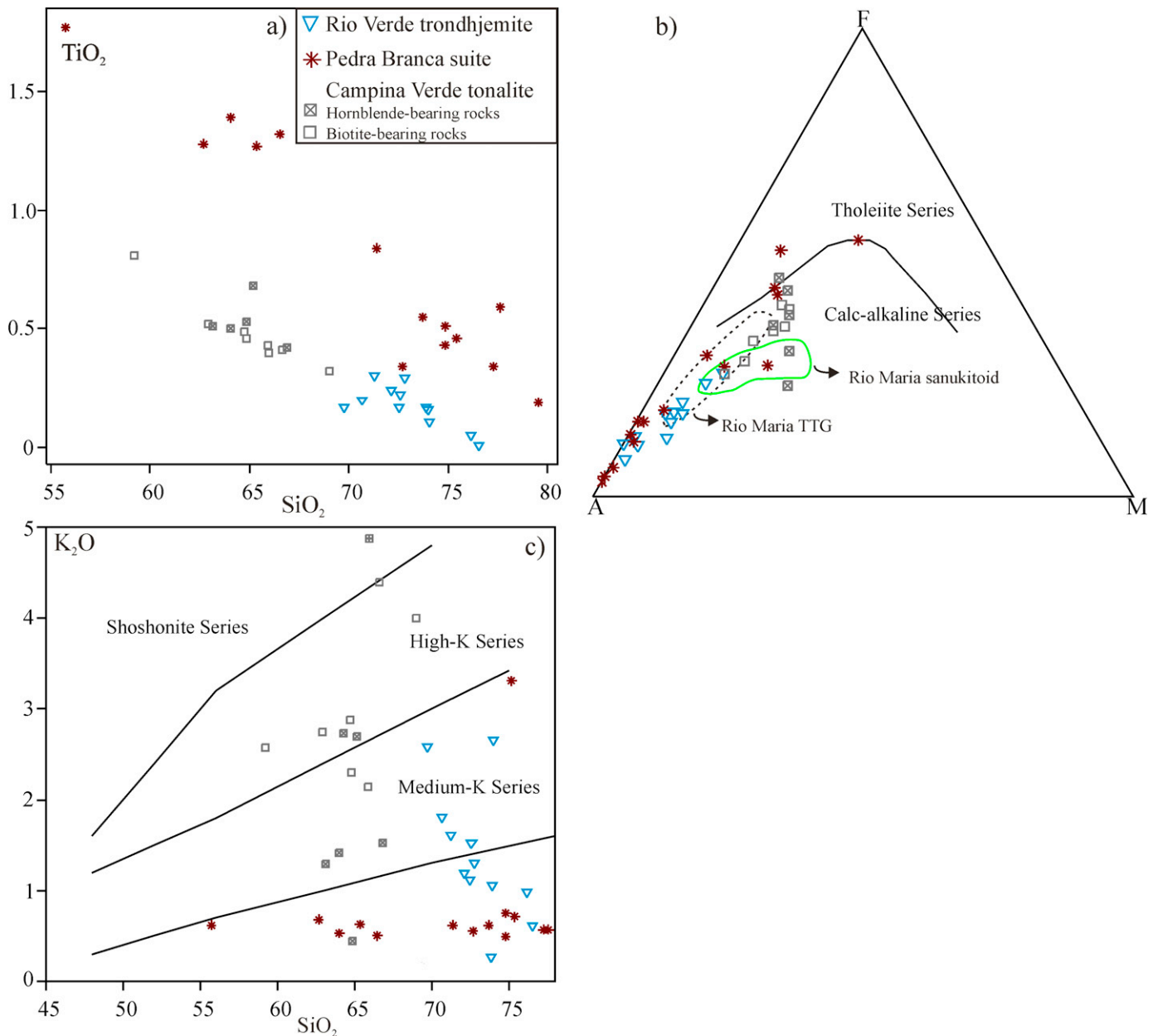


Fig. 5. Geochemical diagrams of the tonalitic-trondhjemitic units of the Canaã area: (a) SiO_2 vs. TiO_2 diagram; (b) AFM diagram (fields of tholeiite and calc-alkaline series of Irvine and Baragar, 1971); (c) K_2O vs. SiO_2 diagram (fields of Peccerillo and Taylor, 1976).

granite units are distinguished for their variable Rb/Sr ratios or, in the case, of the Bom Jesus and Canaã dos Carajás granites, also for their contrast in Zr contents. The Planalto and Bom Jesus granites are also distinguished, respectively, by their lowest and highest La/Yb and Sr/Y ratios compared to the other units (Fig. 7b). These show similar Sr/Y but distinct La/Yb which increases from the Canaã dos Carajás to the Serra Dourada and attains maximum values in the Cruzadão granite. In the La/Yb vs. Eu/Eu^* diagram (Fig. 7c), it can be seen that the Canaã dos Carajás and Bom Jesus granites have relatively higher Eu/Eu^* values when compared to the other granite units. This reflects the discrete or absent Eu anomalies observed in the former granites and the moderate to accentuated negative Eu anomalies shown by the Planalto, Serra Dourada and Cruzadão granites (Fig. 7d). Besides the contrast in the Eu anomalies, the studied granites differ also by their distinct $(\text{La}/\text{Yb})_N$ ratios and total REE contents (Fig. 7b–d; Table 2).

5. Pb-evaporation and U–Pb LA-MC-ICPMS on zircon geochronology

5.1. Introduction

The available geochronological data on the Archean granitoids of the Carajás domain, including the ‘Transition’ sub-domain and the Canaã dos Carajás area, as well as the new ages obtained in this work are in Table 4. We have studied representative samples of the Rio Verde trondhjemite (AER-11A and GRD-79C), Campina Verde tonalitic complex (ARC-65A, ERF-07C, and ARC-95A), Pedra Branca suite (AMR-191A), and Canaã dos Carajás (AMR-102), Bom Jesus (GRD-47), Cruzadão granite (ARC-100 and GRD-58), Serra Dourada granite (GRD-59), and Planalto suite (ARC-109 and AMR-187B) granites. The geochronological/isotopic methods (U–Pb LA-MC-ICPMS, zircon evaporation dating and Sm–Nd isotope systematic)

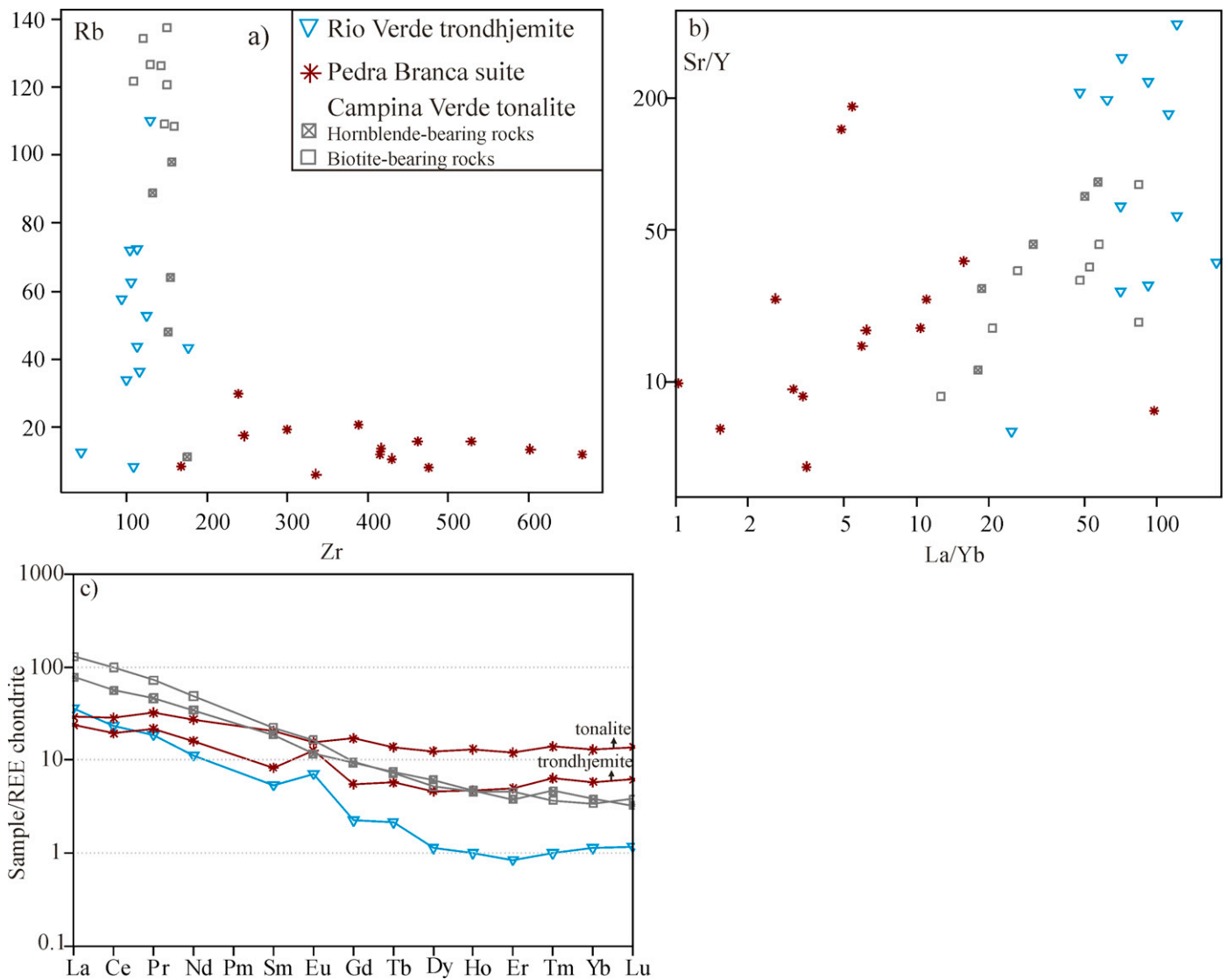


Fig. 6. Trace element diagrams of the tonalitic-trondhjemitic units of the Canaã area: (a) Zr vs. Rb diagram; (b) La/Yb vs. Sr/Y diagram; (c) chondrite normalized REE patterns (Nakamura, 1974).

are described in Appendix B and the isotope data are presented in supplementary Tables A–C.

5.2. Rio Verde trondhjemite

Two samples of biotite trondhjemite (AER-11) and biotite granodiorite (GRD-79C) were both dated by the Pb-evaporation on zircon and U–Pb LA-MC-ICPMS methods.

Twelve zircon grains of AER-11 were analyzed by Pb-evaporation and three grains (Fig. 8a; Table A) yielded an age of 2929 ± 3 Ma (MSWD = 3.0). Forty-two analyses on twenty-six zircons were performed by the U–Pb LA-MC-ICPMS method. Most analyses were strongly discordant and were discarded. Reducing the degree of discordance to a maximum of 3%, seven spots in different zircon grains (Fig. 9a; Table B) defined a concordia age of 2923 ± 15 (MSWD = 6.8). This age is similar to that obtained by the Pb-evaporation method.

Eleven zircon grains of GRD-79C were analyzed by Pb-evaporation and four grains (Fig. 8b) gave an age of 2868 ± 4 Ma (MSWD = 1.13). Forty spot analyses on twenty-five zircon grains were performed by the U–Pb LA-MC-ICPMS method. Almost all analyses are strongly discordant and do not define a clear age.

One concordant analyzed zircon yielded an age of 2841 ± 9 Ma (MSWD = 2.4) and the spot analyses aligned with that grain (Fig. 9b) gave an upper intercept age of 2820 ± 22 Ma (MSWD = 4.8). The age obtained by the Pb-evaporation method is slightly older than that indicated by the concordant zircon grain (U–Pb LA-MC-ICPMS method).

5.3. Campina Verde tonalitic complex

Two samples of the Campina Verde tonalitic complex representative of the biotite tonalite to granodiorite and biotite-hornblende tonalite varieties were selected for dating, a biotite granodiorite (ERF-7C) collected along the road between Vila Planalto and Parauapebas (Fig. 2) and a biotite-hornblende tonalite (ARC-65A) from a quarry located at ca. 1 km to the west of Vila Planalto. A third sample of the biotite-hornblende tonalite (ARC-95) associated with the Cruzadão granite, located to the west of the Rio Branco granite (Fig. 2), was also dated.

The biotite granodiorite (ERF-7C) was dated only by the Pb-evaporation method. Twelve zircon crystals were analyzed and five of them (Fig. 8c; Table A) defined a mean age of 2868 ± 2 Ma (MSWD = 1.3).

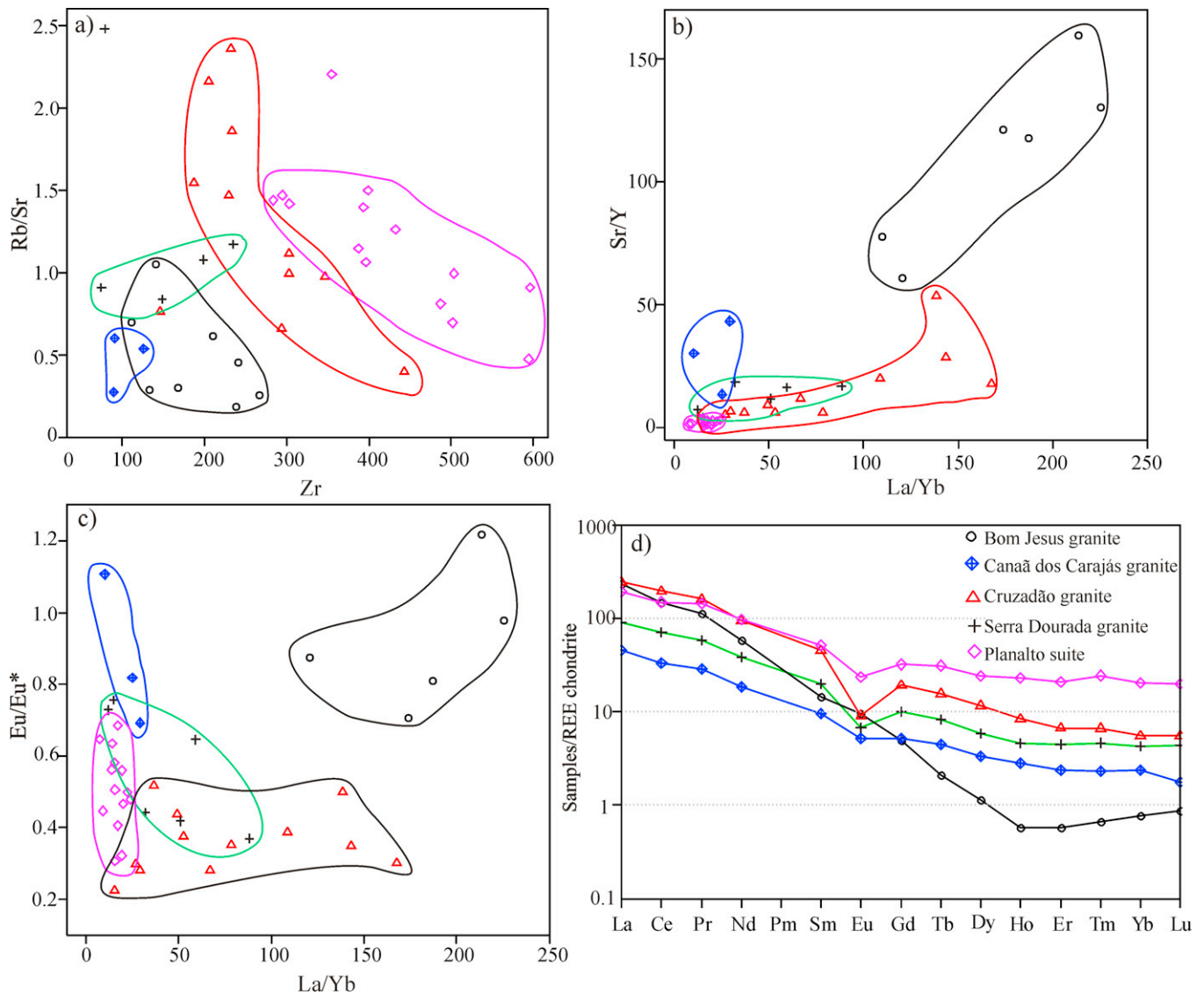


Fig. 7. Trace element diagrams of the Archean granites of the Canaã area: (a) Zr vs. Rb/Sr; (b) La/Yb vs. Sr/Y; (c) La/Yb vs. Eu/Eu*; and (d) REE patterns of representative selected samples of the different granite units.

The biotite-hornblende tonalite (ARC-65A) was dated by the Pb-evaporation method. Fourteen crystals were analyzed and five were used to calculate a mean age of 2872 ± 1 Ma (MSWD = 1.2; Fig. 8d; Table A). The same sample was also analyzed by the U-Pb LA-MC-ICPMS method. Eliminating all spots analyses with discordance greater than 3% of discordance, the remaining nine spot analyses yielded a concordant age of 2850 ± 7 Ma (MSWD = 2.7; Fig. 9c; Table B). That age is younger than the Pb-evaporation age. Three analyzed spots in the outer zone of zircon grains yielded an age of 2724 ± 15 Ma (MSWD = 3.0), probably due to Pb-loss related to the opening of the U-Pb system during an event of Neoproterozoic age. One analyzed zircon grain, interpreted as inherited, provided the age of 3002 ± 23 Ma (MSWD = 1.6).

Sample ARC-95 was also dated by the Pb-evaporation and U-Pb LA-MC-ICPMS methods on zircon. Fifteen zircon crystals were analyzed by Pb-evaporation and six of them defined a mean age of 2853 ± 2 Ma (MSWD = 3.1; Fig. 8e; Table A). One analyzed zircon provided an age of 2966 ± 5 Ma and most likely represents an inherited grain. Twenty-three zircon grains were analyzed by the U-Pb LA-MC-ICPMS method. Reducing the degree of discordance

to a maximum of ~10%, the twelve remaining spots defined an upper intercept age of 2851 ± 18 Ma (MSWD = 2.9) and eight concordant analyses (Fig. 9d) gave a concordia age of 2849 ± 18 Ma (MSWD = 0.13). An isolated zircon grain yielded a concordia age of 2647 ± 23 Ma (MSWD = 0.047).

The ages obtained in this work for the different dated samples of the Campina Verde tonalitic complex comprised between 2.87 Ga and 2.85 Ga and this interval is assumed as the crystallization age for that granitoid. The sample ARC-95 is associated with the Cruzadão granite which, in the later stages of its evolution, was apparently deformed simultaneously with that tonalite.

5.4. Canaã dos Carajás granite

A biotite leucomonzogranite (sample AMR-102) of the Canaã dos Carajás granite was dated by the Pb-evaporation method (ca. 2.93 Ga; Sardinha et al., 2004). Additional LA-MC-ICPMS dating was performed in the same sample. Twenty-one zircon grains were analyzed and, when possible, analyses of core and border zones were

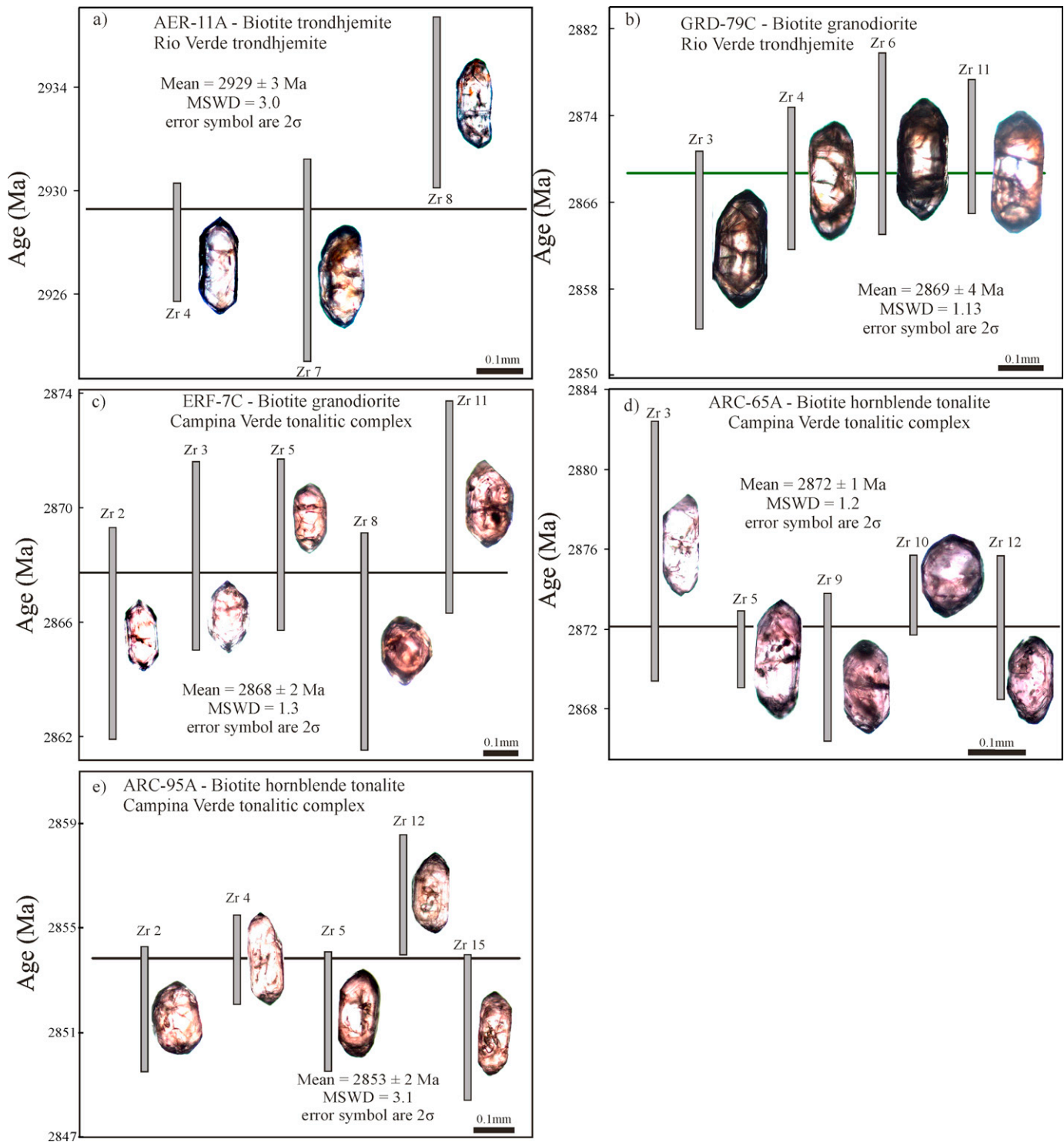


Fig. 8. Single zircon Pb-evaporation age diagrams for the granitoids of the Canaã area: (a) Rio Verde trondhjemite (AER-11A); (b) Rio Verde trondhjemite (GRD-79C); (c) biotite granodiorite (ERF-7C), (d) biotite-hornblende tonalite (ARC-65A), and (e) biotite-hornblende tonalite (ARC-95A) of the Campina Verde tonalite. The vertical bar represents the error for each zircon grain and horizontal thick line corresponds to the mean age for the dated samples.

performed in the same grain. The obtained results are shown in Table B and Fig. 9e. Most analyses show high discordance or large errors, and were therefore not used in the age calculation. Seven analyses obtained in five grains resulted in an upper intercept age of 2952 ± 24 Ma (MSWD = 2.3). Using only analytical results with discordance smaller than 3%, the remaining five analyses in four distinct zircon grains plot on the concordia curve and yielded an age of 2959 ± 6 Ma (MSWD = 1.5). This age is slightly older than

the Pb-evaporation age and is interpreted as the crystallization age of the Canaã dos Carajás granite. A zircon core gave a concordia age of 3030 ± 15 Ma (MSWD = 1.3) and was interpreted as an inherited grain. Another concordant zircon yielded a concordia age of 2864 ± 12 Ma (MSWD = 1.2), probably due to an opening of the U–Pb system. The presence of an older inherited zircon in the dated rock indicates a probable crustal source for the magma of this granite. The younger age of ca. 2.86 could be related to reworking

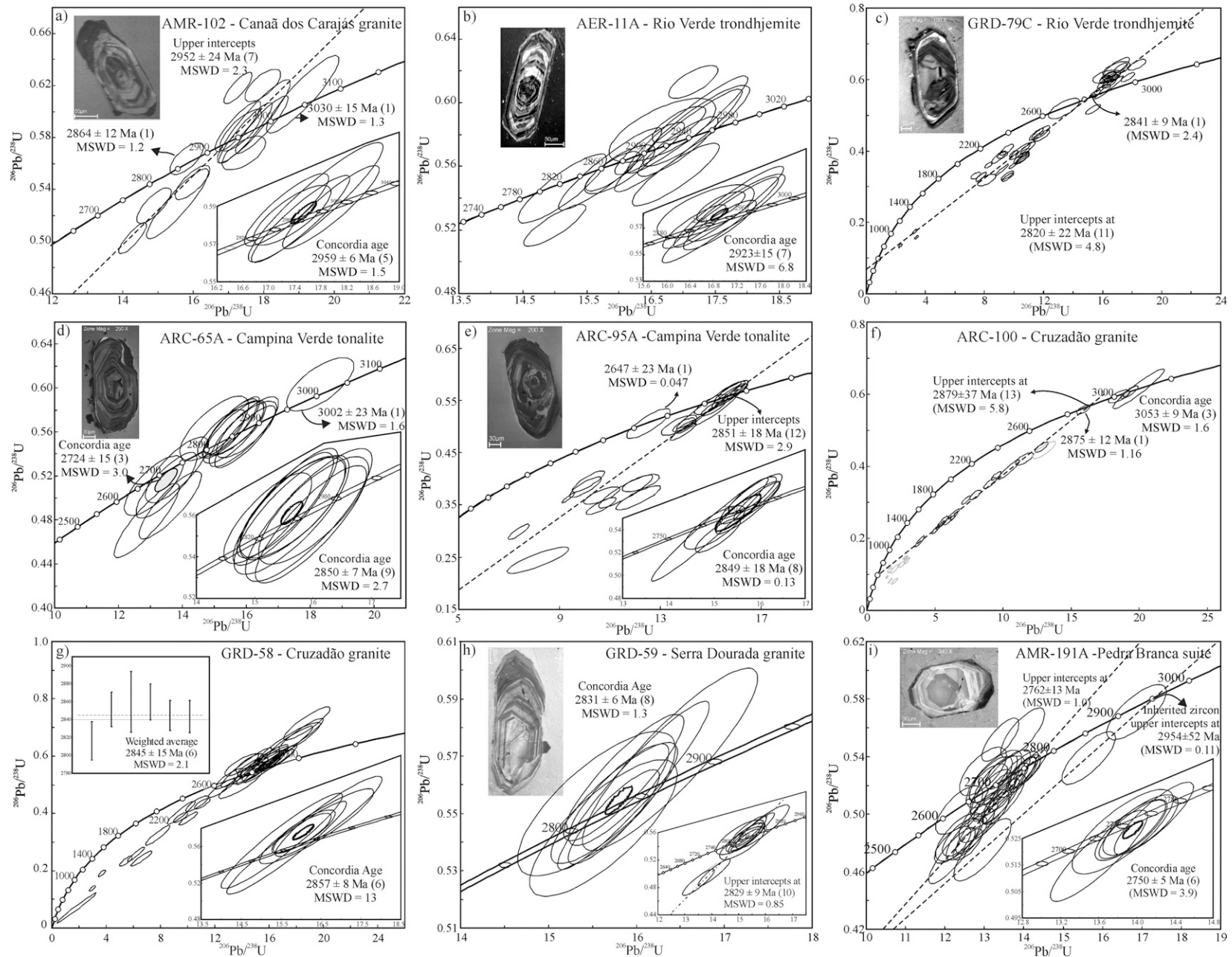


Fig. 9. LA-MC-ICPMS U–Pb concordia diagram for the samples of the Archean granitoids of the Canaã area: (a) Rio Verde trondhjemite (AER-11A); (b) Rio Verde trondhjemite (GRD-79C); (c) Campina Verde tonalitic complex (ARC-65A); (d) Campina Verde tonalitic complex (ARC-95A); (e) Canaã dos Carajás granite (AMR-102); (f) Cruzadão granite (ARC-100); (g) Cruzadão granite (GRD-58); (h) Serra Dourada granite (GRD-59); and (i) Pedra Branca suite (AMR-191A).

of the granite during the important magmatic and tectonic events identified in the Canaã area at that time (cf. Table 4).

5.5. Bom Jesus granite

A biotite leucosyenogranite (GRD-47) of the Bom Jesus granite was dated by the U–Pb LA-MC-ICPMS method and the obtained results (Table B) show that most analyzed spots are strongly discordant. Discarding grains with more than 5% of discordance the remaining grains are still extremely dispersed in the age diagram and did not define a unique age for this granite. Several analyzed spots are disposed near the concordia curve but they are dispersed and isolated grains define extremely variable ages: 3005 ± 15 Ma (MSWD=0.15), 2963 ± 13 Ma (MSWD=1.8), 2914 ± 14 Ma (MSWD=1.5), 2847 ± 13 Ma (MSWD=1.6), 2699 ± 11 Ma (MSWD=0.71), 2588 ± 15 Ma (MSWD=1.3).

Owing to the complexity of the results obtained by the U–Pb LA-MC-ICPMS method, it was decided to date this sample also by the U–Pb SHRIMP technique. Ten analyzed zircon grains (Table C) provided an upper intercept age of 2833 ± 6 Ma (MSWD=1.8; 1σ) with two grains yielding ages of 3017 ± 5 Ma and 3074 ± 6 Ma (Fig. 10a). The lower intercept defined an age of 525 ± 44 Ma possibly related to uplift of the Canaã area or to the formation of the Araguaia belt, during the Brasiliano cycle (Fig. 1).

5.6. Cruzadão granite

Two samples of the Cruzadão granite were selected for dating by the U–Pb LA-MC-ICPMS method. Sample ARC-100 (biotite leucosyenogranite) is located in the western and GRD-58 (biotite syenogranite) in the central-southern exposed area of that granitic unit.

The 21 analyzed zircon grains of ARC-100 show with a few exceptions a high degree of discordance. Using only analyses that are less than 50% discordant, the thirteen remaining zircon grains (Fig. 9f) define an upper intercept age of 2879 ± 37 Ma (MSWD=5.8) and one isolated grain yielded a 2875 ± 12 Ma (MSWD=1.16) concordia age. Three grains gave an older concordia age of 3056 ± 9 Ma (MSWD=1.6). In the sample GRD-58, twenty-five zircon grains were analyzed. Eliminating the most discordant grains, 16 remaining spot analyses (Fig. 9g) did not define an upper intercept age. However, the six zircon analyses with less than 5% discordance gave a concordia age of 2857 ± 8 Ma (MSWD=13). These same six grains yielded a mean weighted average $^{207}\text{Pb}/^{206}\text{Pb}$ age of 2845 ± 15 Ma (MSWD=2.1). Other three zircon grains with low-discordance yielded a concordia age of 2785 ± 16 Ma (MSWD=4.1).

5.7. Serra Dourada granite

A biotite leucomonzogranite (GRD-59) of the central area of the Serra Dourada pluton (Fig. 2) was sampled for dating.

Fifty-five U–Pb LA-MC-ICPMS analyses performed on thirty-one zircon grains yielded in general strongly discordant analytical points (Table B). Eight zircon grains (Fig. 9e) provided a concordia age of 2831 ± 6 Ma (MSWD=1.3).

This age is slightly younger than the upper intercept age of 2860 ± 22 Ma (MSWD=11.5) obtained for the same granite unit (Moreto et al., 2011), but both ages are almost superposed within errors. The fact that the age presented in this work is a concordia age with a relatively low MSWD makes it more reliable and it is interpreted as the crystallization age of the Serra Dourada granite.

5.8. Pedra Branca suite

Sample AMR-191 (trondhjemite) of this suite was selected for LA-MC-ICPMS study.

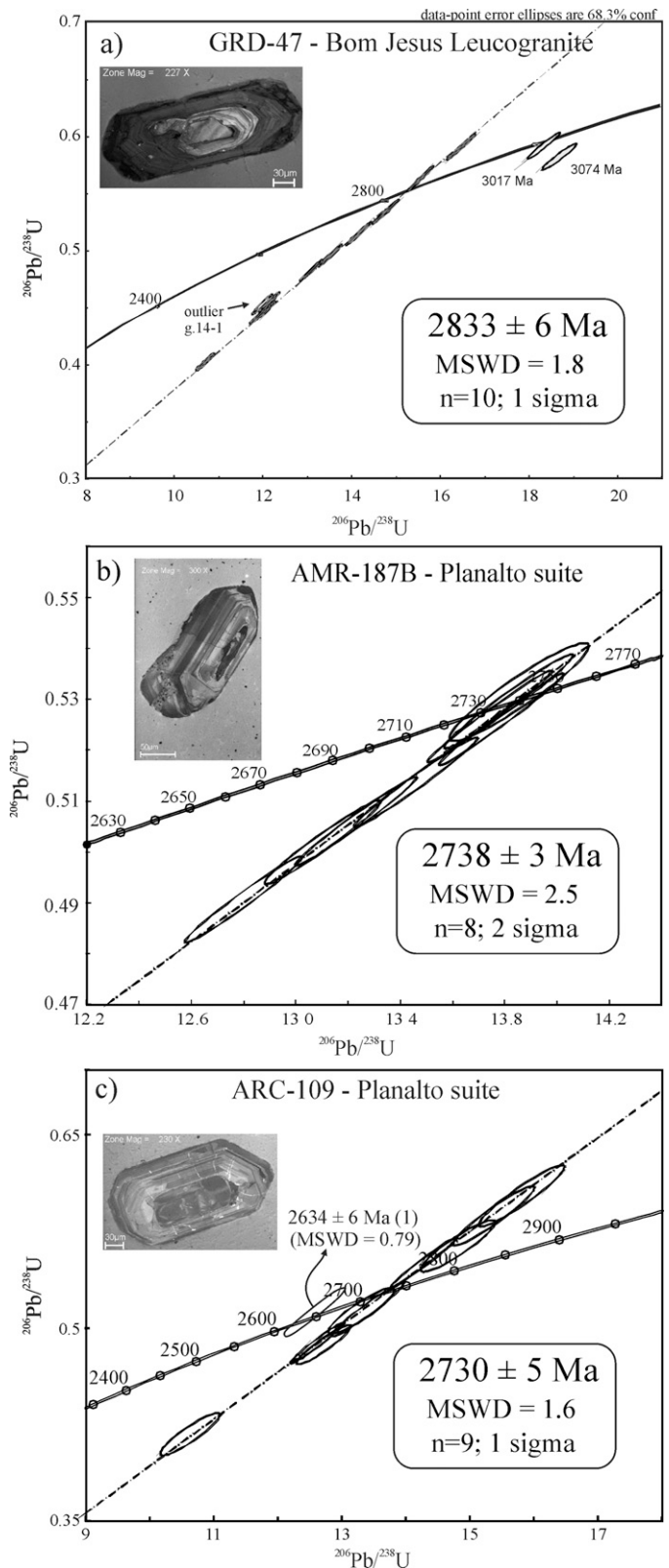


Fig. 10. Concordia plot showing SHRIMP U–Pb zircon data. (a) Bom Jesus granite (GRD-47); (b) Planalto suite (AMR-187B); (c) Planalto suite (ARC-109).

Twenty-nine zircon grains were analyzed by LA-MC-ICPMS and, when possible, analyses of core and rims were performed in the same grain. The obtained results are shown in Table B and Fig. 9i. The zircon analyses show a complex distribution in the concordia diagram and a significant number of analyzed spots is discordant (Fig. 9i). In a preliminary approach, the analyses with more than 10% of discordance were discarded and the remaining data yielded an upper intercept age of 2762 ± 13 Ma (MSWD = 1.0; Fig. 9i). Reducing the discordance to a maximum of 2.5%, 6 zircon analyses, performed in core and border zones and in bright and darker zones of the crystals, gave a concordia age of 2750 ± 5 Ma (MSWD = 3.9; Fig. 9i). Three zircon grains similar to those of the dominant population yielded an upper intercept age of 2954 ± 52 Ma (MSWD = 0.11) and were interpreted as inherited zircons. There are several analyses that suggest younger ages but they do not define a precise age.

5.9. Planalto suite

The available geochronological data and new dating on this unit (Table 4) were reported by Feio et al. (2012).

Additional U–Pb SHRIMP on zircon ages on two samples (AMR-187B and ARC-109) previously dated by Feio et al. (2012) were obtained in the present work. The analytical procedures are described in Appendix B and isotope data are presented in Supplementary Table C. Sample AMR-187B came from a stock to the east of Canaã dos Carajás town and ARC-109 from another stock in the southwestern part of the study area (Fig. 2). Eight analyzed zircon grains of the sample AMR-187B (Fig. 10b) yielded an upper intercept age of 2738 ± 3 Ma (MSWD = 2.5; 2σ). Sixteen analyses were done on zircon grains of sample ARC-109. Discarding the seven most discordant data (Fig. 10c), it resulted in an upper intercept age of 2730 ± 5 Ma (MSWD = 1.6; 1σ).

6. Sm–Nd isotopic data

The Nd isotope data and the ages assumed for the different units are presented in Table 5. The Sm and Nd contents are quite variable in the different granitoid units. They are relatively low in the analyzed samples (1.2–4.9 ppm of Sm and 10–31 ppm of Nd), except for the Planalto and Cruzadão granites, in the orthopyroxene quartz gabbro and in sample ARC-142 of the Pedra Branca suite, where the Sm and Nd contents are higher (6–17 ppm of Sm and 42–124 ppm of Nd). The $^{147}\text{Sm}/^{144}\text{Nd}$ ratios show strong variations with some granitoids with ratios varying between 0.09 and 0.12 (Canaã dos Carajás, Serra Dourada, Planalto granites, Campina Verde tonalitic complex, orthopyroxene quartz gabbro and the samples GRD-58 of the Cruzadão granite and AMR-191 of the Pedra Branca suite; Table 5) and others with comparatively lower ratios of 0.050–0.075 (Rio Verde trondhjemite, Bom Jesus granite and the samples ARC-113 of the Cruzadão granite and ARC-142 of the Pedra Branca suite).

Among the Mesoarchean units, the Canaã dos Carajás granite and Campina Verde tonalitic complex show a broadly similar behavior of the Sm–Nd isotopic system. The Nd model ages vary from 3162 Ma to 3050 Ma and their $\epsilon\text{Nd}(t)$ values (Table 5) are slightly negative from -0.04 to -4.09 , except for an isolated sample (ERF-07C with T_{DM} of 2944 Ma and ϵNd of +0.94). On the other hand, the $\epsilon\text{Nd}(t)$ values for the Bom Jesus, Cruzadão and Serra Dourada granites are positive (+2.31 and +0.12) with T_{DM} depleted-mantle model ages varying from 2999 Ma to 2932 Ma. The Neoproterozoic granitoids (Planalto and Pedra Branca suites and Charnockitic rock) show T_{DM} varying from 3136 Ma to 2952 Ma and ϵNd is always negative (-0.85 to -2.25 ; Table 5), except for the sample AMR-152 of the Planalto suite (T_{DM} of 2813 Ma and ϵNd of +1.38).

7. Discussion

7.1. Ages of the Archean granitoids of the Canaã area

The new ages obtained for the Archean granitoids of the Canaã area, integrated with those available in the literature, allow us to constrain the timing of the major magmatic events that had taken place in that area (Table 4, Fig. 11). Four major events of rock formation are distinguished: at 3.05–3.0, 2.96–2.93, 2.87–2.83, and 2.75–2.73 Ga (Fig. 12). The 3.05–3.0 Ga event was marked by the formation of the Pium complex and Bacaba tonalite, and by several inherited zircon ages shown by different granitoids (Table 4). During the second event, the crystallization of the Canaã dos Carajás granite and the formation of the older rocks of the Rio Verde trondhjemite took place. During the third stage, the dominant rocks of the Campina Verde tonalitic complex and Rio Verde trondhjemite, as well as Serra Dourada granite were crystallized. The Cruzadão and Bom Jesus granites include zircons with ages varying from 3.05 Ga to 2.83 Ga and had probably a complex evolution. 2.85–2.83 Ga is interpreted as a minimum age for those granites. Finally, the fourth event occurred during the Neoproterozoic when the Planalto and Pedra Branca suites and the charnockites associated with the Pium complex were crystallized.

Three major events of rock formation occurred, therefore, during the Mesoarchean and are not very distinct in age of those registered so far in the Carajás province as a whole. On the other hand, the fourth Neoproterozoic magmatic event identified in Canaã is also present in the Carajás basin but absent in the Rio Maria domain.

The different ages obtained for the Rio Verde trondhjemite (Table 4, Fig. 11) are difficult to interpret. The ~ 2.93 Ga age yielded by the AER-11A sample may suggest the existence of older trondhjemitic rocks associated with the dominant trondhjemites probably aged of 2.87–2.85 Ga. An alternative interpretation would be to admit that the dated zircons of AER-11A were inherited but this hypothesis is not favored because a significant number of spot analyses were employed to define the concordia age (Fig. 9b). It is concluded that the Rio Verde trondhjemite was possibly formed in different periods in between 2.93 and 2.85 Ga.

The evolution of the Bom Jesus and Cruzadão granites was complex as indicated by the ages varying between 3.05 and 2.83 Ga given by zircons of two different populations and evidence of zircon overgrowths (Table 4, Fig. 11). A sedimentary source for these granites would be able to explain the diversity of zircon shape and ages but the geochemical characteristics of these rocks are not consistent with such origin (cf. geochemistry section). At the present moment, the 2833 ± 6 Ma age can be seen as a minimum crystallization age for the Bom Jesus and Cruzadão granites, which could have a polycyclic evolution. The field relationships between the Bom Jesus granite and the Rio Verde trondhjemite suggest that both units were deformed simultaneously in the later stages of their evolution. A similar relationship is shown by the Cruzadão granite and the Campina Verde tonalite.

The Pedra Branca suite also had a complex geologic evolution (Table 4, Fig. 11). This is indicated by the presence of inherited and rejuvenated zircon grains and abundant fractures in the zircon crystals. The ages of the inherited zircons are coincident within errors with important events of the Canaã area crustal evolution (2.96–2.93 Ga). The concordia age of 2750 ± 5 Ma obtained in the dominant zircon population is interpreted as the crystallization age of the Pedra Branca granitoids.

Three samples of the Planalto granite yielded extremely similar Pb–evaporation on zircon ages (ca. 2730 Ma, Table 4, Fig. 11). These ages are a little younger than those of the Planalto suite of its type area (2747 ± 2 Ma, Huhn et al., 1999) and of two stocks located in the ‘Transition’ sub-domain (2754 ± 2 Ma, Silva et al., 2010;

Table 4
Summary of the available geochronological data of the 'Transitional' subdomain and new data obtained in this work.

Units	Rock type	Method	Zircon age (Ma)	Ref.	Characteristics of analyzed zircon crystals	
Cristalino	Diorite	Pb-evaporation	2738 ± 6	1		
Planalto suite	Granite	Pb-evaporation	2747 ± 2	1	Translucent to transparent, prismatic slightly rounded and fractured; pale brown; irregular dark gray cores; rims with oscillatory zoning and locally dark.	
		Hb-Bt monzogranite	Pb-evaporation	2734 ± 2		2
	Bt-Hb sienogranite	Pb-evaporation	2754 ± 2	2		
	Bt-Hb syenogranite/AMR-187B	Pb-evaporation	2733 ± 2	3		
		U-Pb LA-MC-ICPMS	2729 ± 17	3		
		U-Pb SHRIMP	2738 ± 3	9		
	Hb-Bt syenogranite/ARC-109	Pb-evaporation	2731 ± 1	3		
		U-Pb LA-MC-ICPMS	2710 ± 10	3		
		U-Pb SHRIMP	2730 ± 5	9		
	Bt syenogranite/GRD-77	Pb-evaporation	2736 ± 4	3		
U-Pb LA-MC-ICPMS		2706 ± 5	3			
Charnockite association	Opx-trondhjemite Qtz-gabbro	Pb-evaporation	2754 ± 1	2		
		U-Pb LA-MC-ICPMS	2735 ± 5	3		
Estrela Complex Serra do Rabo	Granite Hb syenogranite	Pb-evaporation	2763 ± 7	4		
		U-Pb TIMS	2743 ± 2	4		
Igarapé Gelado	Granite	Pb-evaporation	2731 ± 26	4		
Pedra Branca suite	Trondhjemite Trondhjemite Trondhjemite/AMR-191A	Pb-evaporation	2749 ± 6 ^a	5	Dominant elongated, prismatic (rectangular in section), euhedral or slightly rounded; subordinate short prismatic or rounded. Both light brown, translucent to transparent, intensely fractured and with metamictic cores; overgrowths (?) around corroded cores.	
		U-Pb TIMS	2765 ± 39	5		
		U-Pb LA-MC-ICPMS	2750 ± 5	9		
		U-Pb LA-MC-ICPMS	2954 ± 52 ^b	9		
		U-Pb LA-MC-ICPMS	2701 ± 6 ^c	9		
Serra Dourada granite	Granite Leucomonzogranite/GRD-59	U-Pb LA-MC-ICPMS	2860 ± 22	7	Subhedral, pinkish, elongated, prismatic, slightly rounded, and fractured; oscillatory-zoning.	
		U-Pb LA-MC-ICPMS	2831 ± 6	9		
Cruzadão granite	Bt syenogranite/GRD-58A	U-Pb LA-MC-ICPMS	2845 ± 15	9	Prismatic, light pinkish, and zoned. overgrowths (?) dark; some are rounded; other grains are uniform and darker; partial metamictization and fractures.	
		U-Pb LA-MC-ICPMS	2857 ± 8	9		
		U-Pb LA-MC-ICPMS	2785 ± 16 ^c	9		
		U-Pb LA-MC-ICPMS	2675 ± 26 ^c	9		
		Bt leucosyenogranite/ARC-100	U-Pb LA-MC-ICPMS	2875 ± 12		9
			U-Pb LA-MC-ICPMS	3053 ± 8		9
Bom Jesus gneissic granite	Bt leucosyenogranite/GRD-47	U-Pb SHRIMP	2833 ± 6	9	First population (125–180 μm): Prismatic, light brownish, zoned; overgrowths (?) dark; some are rounded; other grains are uniform and darker; partial metamictization and fractures. Second population (<125 μm): rounded and brownish (shrimp age).	
		U-Pb SHRIMP	3017 ± 5 and 3074 ± 6 Ma ^b	9		
Campina Verde tonalitic Complex	Bt-Hb tonalite/ARC-65A	Pb-evaporation	2872 ± 1	9	Colorless to pale brown subeuhedral short prismatic with rounded edges and few inclusions and fractures. Well-developed oscillatory-zone.	
		U-Pb LA-MC-ICPMS	2850 ± 7	9		
		U-Pb LA-MC-ICPMS	3002 ± 23 ^b	9		
		U-Pb LA-MC-ICPMS	2724 ± 15 ^c	9		
	Bt-Hb tonalite/ARC-95A	Pb-evaporation	2854 ± 2	9		
		Pb-evaporation	2966 ± 5 ^b	9		
		U-Pb LA-MC-ICPMS	2849 ± 18	9		
		U-Pb LA-MC-ICPMS	2868 ± 2	9		
Bacaba tonalite	Tonalite Tonalite Tonalite	U-Pb LA-MC-ICPMS	2997 ± 5	7		
		U-Pb LA-MC-ICPMS	2993 ± 7	7		
		U-Pb LA-MC-ICPMS	3005 ± 8	7		

Table 4 (Continued)

Units	Rock type	Method	Zircon age (Ma)	Ref.	Characteristics of analyzed zircon crystals
Rio Verde trondhjemitite	Bt granodiorite/GRD-79C	U–Pb LA-MC-ICPMS	2820 ± 22	9	Pinkish elongated prismatic; euhedral to subhedral shape or locally rounded. Oscillatory zoning and low luminescence; bright zones in some metamict grain cores.
		U–Pb LA-MC-ICPMS	2709 ± 30 ^c	9	
		Pb-evaporation	2869 ± 4	9	
	Bt trondhjemitite/AER-11A	Pb-evaporation	2929 ± 3	9	
	Bt trondhjemitite/AER-11A	U–Pb LA-MC-ICPMS	2923 ± 15	9	
		U–Pb LA-MC-ICPMS	2868 ± 6 ^c	9	
Canaã dos Carajás granite	Bt leucomonzogranite/AMR-102	Pb-evaporation	2928 ± 1	5	Fractured, translucent to transparent prismatic; slightly rounded edges and brown color. Subordinate short prismatic or rounded. Evidence of inherited cores
	Bt	U–Pb LA-MC-ICPMS	2959 ± 6	9	
	leucomonzogranite/AMR-102	U–Pb LA-MC-ICPMS	3030 ± 15 ^b	9	
		U–Pb LA-MC-ICPMS	2864 ± 12 ^c	9	
Xingu complex	Granodiorite	Pb-evaporation	2852 ± 16	8	
	Granitic leucossoma	U–Pb TIMS	2859 ± 2	8	
	Bt trondhjemitite	Pb-evaporation	2872 ± 2	6	
	Gneiss granodiorite	Pb-evaporation	2974 ± 15	8	
Pium complex	Protolith of the enderbite	U–Pb SHRIMP	3002 ± 14	10	
	Enderbite	U–Pb SHRIMP	2859 ± 9 ^c	10	

Bt, biotite; Hb, hornblende; opx, orthopyroxene; qtz, quartz. Data source: (1) Huhn et al. (1999); (2) Oliveira et al. (2010b); (3) Feio et al. (2012); (4) Barros et al. (2009); (5) Sardinha et al. (2004); (6) Machado et al. (1991); (7) Moreto et al. (2011); (8) Avelar et al. (1999); (9) this work; (10) Pidgeon et al. (2000).

^a Recalculated age for 2 sigma.

^b Inherited zircon.

^c Opening of the isotopic system or metamorphism.

Table 5
Sm–Nd isotopic data for the granitoids of the Canaã dos Carajás area.

Sample	Sm (ppm)	Nd (ppm)	¹⁴⁷ Sm/ ¹⁴⁴ Nd	¹⁴³ Nd/ ¹⁴⁴ Nd ($\pm 2\sigma$)	f(Sm/Nd)	ϵ Nd(0)	ϵ Nd(t)	T _{DM} (Ma)
2.95 Ga Canaã dos Carajás granite								
AMR-102	1.94	11.14	0.1050	0.51082 (6)	–0.4661	–35.46	–0.66	3162
AMR-213	3.84	23.49	0.0988	0.510691 (5)	–0.4977	–37.98	–0.51	3162
2.93 Ga Rio Verde Trondhjemite								
AER-11	1.78	18.70	0.0572	0.509949 (22)	–0.7092	–52.5	0.19	3042
AER-77B	2.55	21.17	0.0741	0.510399 (17)	–1.0000	–43.7	2.61	2913
2.86 Ga Rio Verde trondhjemite								
GRD-79C	1.21	10.08	0.0723	0.510421 (12)	–0.4977	–43.2	2.75	2850
2.85 Ga Campina Verde tonalitic complex								
AER-29A	3.21	17.47	0.1111	0.511008 (8)	–0.4352	–31.80	–0.38	3064
ARC-65A	4.98	31.65	0.0951	0.510651 (9)	–0.5165	–38.76	–1.48	3113
ARC-95A	4.44	23.74	0.1131	0.511033 (13)	–0.4250	–31.31	–0.63	3088
ERF-113	3.75	19.03	0.1192	0.511178 (14)	–0.3940	–28.48	–0.04	3050
ERF-07C	2.48	16.47	0.0910	0.510697 (22)	–0.5374	–37.86	0.94	2944
ERF-134	4.90	29.04	0.1021	0.51065 (26)	–0.4809	–38.78	–4.09	3321
2.85 Ga Cruzadão granite								
ARC-113	7.68	70.78	0.0655	0.510217 (14)	–0.6670	–47.2	2.31	2932
GRD-58A	13.33	82.55	0.0976	0.510793 (1)	–0.5038	–36.0	0.38	2987
2.85 Ga Bom Jesus gneiss granite								
AE-47	1.45	12.04	0.0729	0.510337 (19)	–0.6294	–44.9	0.55	2957
ARC-116	2.6	31.0	0.0508	0.509899 (17)	–0.7417	–53.4	0.12	2967
2.83 Ga Serra Dourada granite								
AER-27	3.02	16.85	0.1084	0.510996 (16)	–0.4489	–32.03	0.15	2999
AER-59	3.47	22.22	0.1025	0.510925 (11)	–0.4789	–33.42	0.92	2935
2.75 Pedra Branca suite								
AMR-191A	1.72	8.94	0.1164	0.51107 (6)	–0.4085	–30.59	–2.16	3136
ARC-142	12.84	124.27	0.0625	0.510141 (7)	–0.6823	–48.71	–1.21	2952
2.73 Ga Orthopyroxene-quartz gabbro								
GRD-05 ^a	11.78	64.64	0.1102	0.51099 (7)	–0.4398	–31.97	–1.59	3049
2.73 Ga Planalto suite								
ARC-108 ^a	6.02	42.00	0.0867	0.510573 (9)	–0.5592	–40.28	–1.64	2996
ARC-109 ^a	11.35	63.00	0.1089	0.511013 (7)	–0.4464	–31.70	–0.85	2988
AMR-152 ^a	13.82	77.83	0.1073	0.511098 (12)	–0.4545	–30.04	1.38	2813
AMR-187B ^a	17.09	100.52	0.1027	0.510901 (17)	–0.4779	–33.88	–0.86	2975
GRD-77 ^a	13.40	77.29	0.1048	0.510868 (23)	–0.4672	–34.53	–2.25	3084

^a Feio et al. (2012).

2748 \pm 2 Ma and 2749 \pm 3 Ma, Souza et al., 2010), all dated by the Pb–evaporation method. The Estrela complex, the Igarapé Gelado and the Serra do Rabo plutons of the Carajás domain, which are geochemically similar to the Planalto suite, yielded, respectively, zircon ages of 2763 \pm 7 Ma and 2731 \pm 26 Ma (Pb–evaporation; Barros et al., 2009) and of 2743 \pm 2 Ma (U–Pb TIMS age; Sardinha et al., 2006). Additional ages were obtained for three distinct plutons of the Planalto suite by the U–Pb LA-MC-ICPMS method (Feio et al., 2012). It resulted in concordia ages of 2729 \pm 17 Ma (AMR-187B), 2710 \pm 10 Ma (ARC-109), and 2706 \pm 5 Ma (GRD-77).

The new ages obtained in the present work for sample AMR-187B are almost coincident within error with those yielded by the Pb–evaporation on zircon and U–Pb LA-MC-ICPMS methods (Feio et al., 2012). The same is true in the case of the Pb–evaporation on zircon and U–Pb SHRIMP on zircon ages of the sample ARC-109. However, the U–Pb LA-MC-ICPMS zircon age obtained for that sample (Feio et al., 2012) is slightly younger. Comparing the different results obtained, it is concluded that the crystallization of the Planalto suite took place between 2740 and 2730 Ma.

7.2. Geochemical signature of the Archean granitoids of the Canaã area: geologic and tectonic implications

The granitoid magmatism identified in the Canaã area is diversified in age and geochemical signature. Two groups of units were recognized: the tonalitic–trondhjemitic units and the granitic ones. The dominantly tonalitic–trondhjemitic units show clear geochemical contrasts that point for their independent origin. The Campina Verde tonalitic complex and the Pedra Branca suite do not have geochemical affinity with TTG suites such as those of the Rio Maria domain (Almeida et al., 2011) or other Archean cratons (Martin,

1994; Smithies, 2000; Condie, 2005; Moyen and Stevens, 2006; Clemens et al., 2006). The Pedra Branca suite is enriched in TiO₂, Zr (Figs. 5a and 6a), and Y and the Campina Verde tonalitic complex defines an expanded magmatic series that has affinity with calc-alkaline series (Figs. 4c and 5b). Only the Rio Verde trondhjemite shows similarities with the TTG suites (Fig. 4c) but its areal distribution is relatively limited in Canaã (Fig. 2), when compared to the observed in the adjacent Rio Maria domain, where TTG units cover large areas. Thus, it is concluded that the TTG magmatism is far more limited in Canaã than in classical Archean terranes. Also relevant is the absence in Canaã of sanukitoid suites (Fig. 2). The latter are common in the later stages of evolution of many Archean cratons (Stern and Hanson, 1991; Smithies and Champion, 2000; Halla, 2005; Lobach-Zhuchenko et al., 2005; Heilimo et al., 2011) and are widespread in the Rio Maria domain (Althoff et al., 2000; Oliveira et al., 2009a, 2010a).

On the other hand, the granitic units, which constitute the second geochemical group, are diversified in age and geochemical signature and occupy large areas in Canaã (more than 60% of the surface covered by granitoids). All granite units are formed essentially by monzogranites and syenogranites and except for the Serra Dourada granite, the other granite units are strongly deformed, showing penetrative foliation and sometimes lineation and folded structures. The Mesoarchean granite units encompass the Canaã dos Carajás, Serra Dourada, Bom Jesus granites, which have affinity with evolved Archean calc-alkaline granites, and the Cruzadão granite that is transitional between calc-alkaline and alkaline (Sylvester, 1994; cf. our Fig. 4f). The Neoproterozoic granites are represented by several granitic stocks that constitute the Planalto suite, which has a ferroan and accentuated alkaline character and is thus distinct from the Mesoarchean

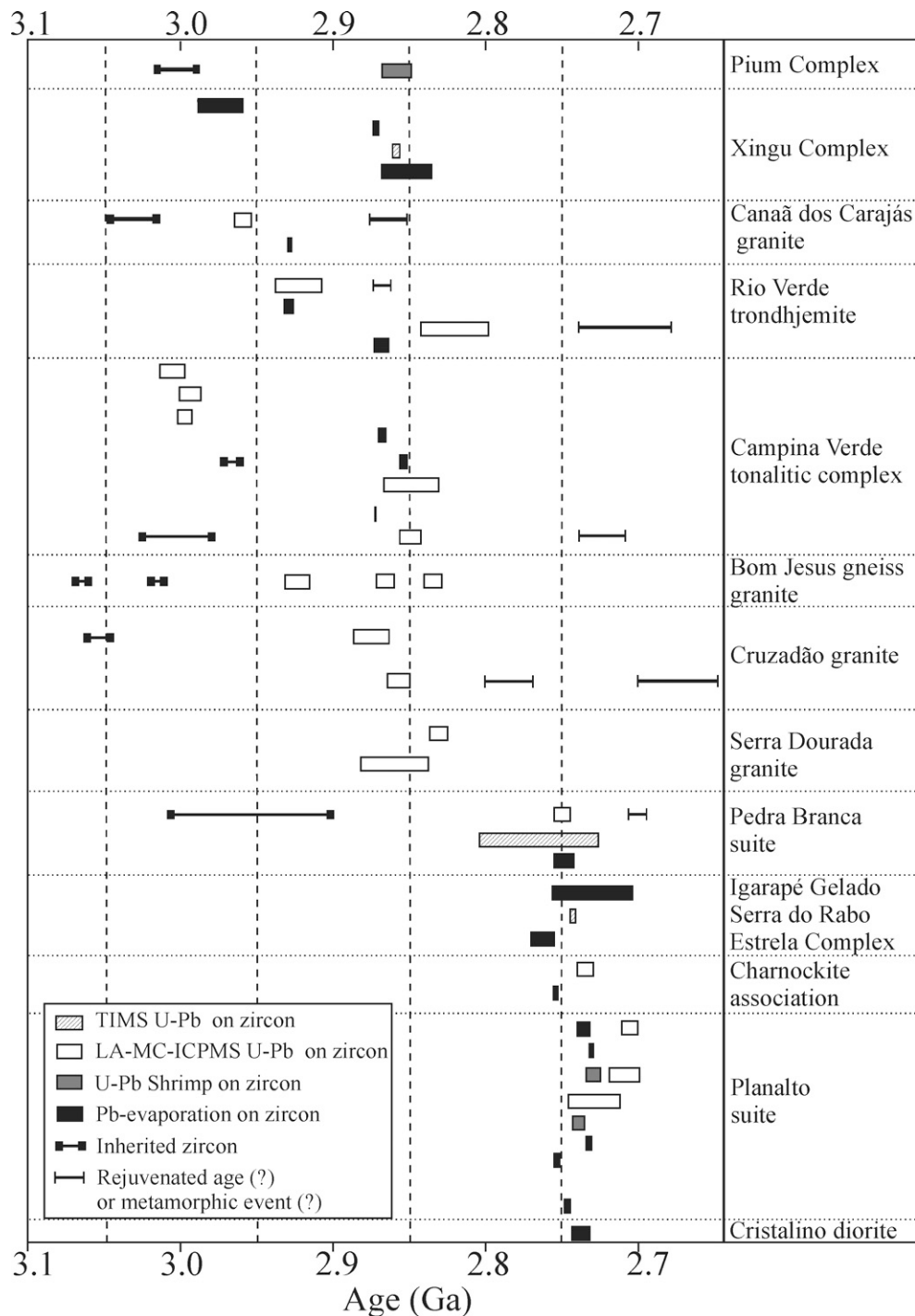


Fig. 11. Summary of geochronological data of the 'Transitional' subdomain available in the literature (data source are given in Table 2), including the new data obtained in this study.

granites found in the same area in age and geochemical signature (Figs. 4e, f and 5a, d; Feio et al., 2012). Neoproterozoic granites similar to those of the Planalto suite are also common in the Carajás basin, being represented by the Estrela complex and the Serra do Rabo and Igarapé Gelado plutons (Sardinha et al., 2006; Barros et al., 2009), and in other areas of the 'Transition' sub-domain to the south of the studied area (Oliveira et al., 2010b).

The dominance of granites (stricto sensu), the absence of sanukitoids and the scarcity of typical TTGs in Canaã demonstrate that

the magmatic series present in that area are very distinct of those of the Rio Maria domain and do not favor a common tectonic evolution for both terranes, even if their Mesoproterozoic rocks have similar ages. Typical Archean terranes are dominated by TTG and greenstone belts with subordinate volumes of sanukitoid and granite rocks (Goodwin, 1991; Condie, 1993; Sylvester, 1994; Jayananda et al., 2006). Granites s.s. are commonly formed in the later stages of evolution of Archean terranes and are generally associated with the stabilization of the oldest cratons (Nisbet, 1987; Kröner, 1991; Davis et al., 1994; Jayananda et al., 2006). Thus, the larger

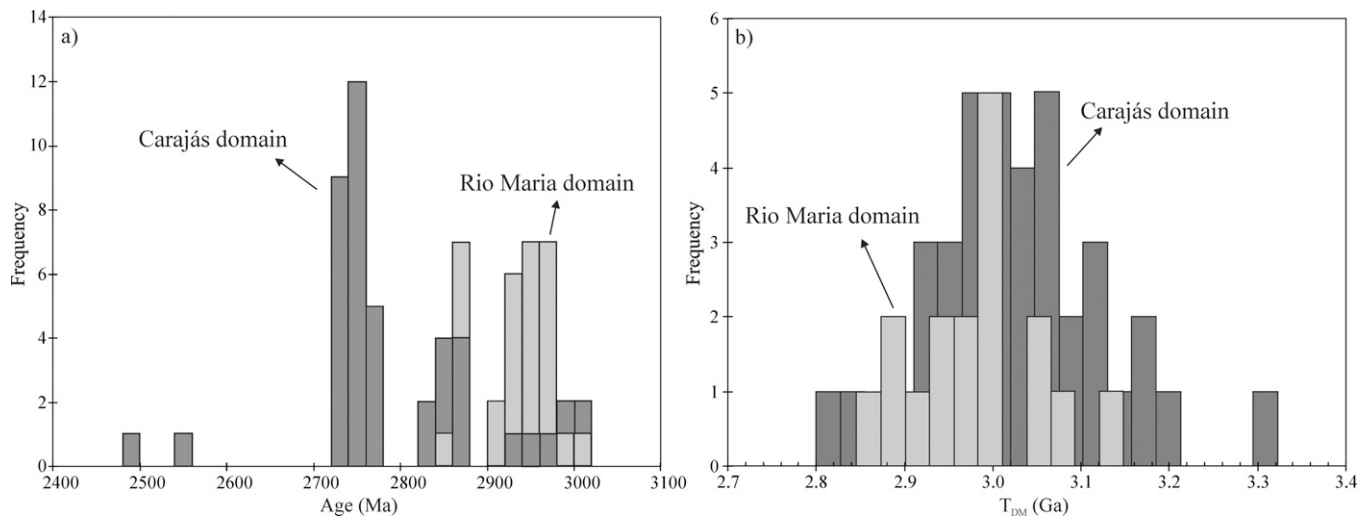


Fig. 12. Histograms of frequency showing (a) the crystallization ages and (b) the depleted mantle (T_{DM}) ages obtained for the Archean rocks of the Carajás and Rio Maria domains, of the Carajás province.

abundance of granitic rocks in Canaã suggests that the Archean crust of that area and possibly also of the 'Transition' sub-domain is not a dominant juvenile character (Fig. 12), and possibly derived from older sialic crust that was tending to stabilization during the Mesoarchean. This is reinforced by the Nd isotope data (see below). The Planalto suite records a remarkable magmatic and deformational Neoproterozoic event that intensely affected the Mesoarchean crust of the Carajás domain and was responsible for the generation of relatively large volumes of ferroan granites associated with charnockite series. This magmatism is a peculiar feature of Canaã and of the entire Carajás domain, which has no equivalent in the Rio Maria domain.

7.3. Crustal evolution of the Canaã area: implications for the Carajás province

The data presented here are not conclusive in relation to the evolution of the 'Transition' sub-domain of the Carajás domain, but they establish some constraints and allow some preliminary conclusions. Geochronological and Nd isotope data (Fig. 12a and b) indicate that the crust of the Canaã area existed at least since the Mesoarchean (ca. 3.2–3.0 Ga) and was strongly reworked during the Neoproterozoic (2.75–2.70 Ga). Differently from the Rio Maria domain where rocks have crystallization ages between 2.98 and 2.86 Ga and show similar Nd T_{DM} ages which is an evidence of their juvenile character, the dated rocks of the Carajás domain show more variable crystallization and also T_{DM} ages. Moreover, the T_{DM} ages of the Canaã granitoids are significantly older than those of Rio Maria, extending to ca. 3.2 Ga (Fig. 12b) and ϵNd values are commonly negative, although positive values have been obtained in the case of some granite units, possibly derived from juvenile crustal sources with short crustal residence times. Besides, the presence of many granitic units in Canaã formed during the Mesoarchean and with ages varying between 2.96 and 2.83 Ga also suggests the existence in Canaã of a continental crust older than that of Rio Maria.

It is probable that a terrane similar to that represented by the Canaã Mesoarchean crust or even an extension of it was the basement of the Carajás basin that was formed during the Neoproterozoic. The tectonic events responsible for the origin of the Carajás rift and the subsequent formation of the Carajás basin and the compressional stage that followed it, both occurring in a short period during the Neoproterozoic, were also registered in the Canaã area. The intense magmatic activity responsible for the origin of the Pedra Branca and

Planalto suite and charnockite rocks and the main deformational structures shown by these units are related to this major tectono-magmatic event. These rocks show penetrative foliation and local subvertical lineation and were affected by thrust faults. This indicates that they were emplaced in a transpressional regime (Fossen and Tikoff, 1998) related to the regional Neoproterozoic deformation that affected the Carajás domain (Pinheiro and Holdsworth, 1997). This Neoproterozoic event is not registered in the Rio Maria domain in the southern part of the Carajás province (Fig. 12a).

The available data on the Carajás domain allow us to evaluate the hypothesis of existence of a 'Transition' sub-domain in between the Rio Maria domain and the Carajás basin (Dall'Agnol et al., 2006). In other words, we should evaluate whether the Canaã crust might correspond to an extension of the Rio Maria domain which has been strongly reworked during the Neoproterozoic. Despite the reasonable coincidence in ages between the Mesoarchean rocks of Canaã and Rio Maria, it is demonstrated that the Rio Maria evolution was concentrated in a shorter period of time (Fig. 12a). Additionally, the contrast in dominant lithologies and Nd isotope behavior (Fig. 12b) between these terranes is remarkable and point to distinct evolution for both. In the $\epsilon Nd(t)$ vs age diagram (Fig. 13), the contrasts between the Archean rocks of Rio Maria and Canaã, including the subalkaline granites of the Carajás basin can be observed more clearly. The evolution paths defined by the rocks of these two domains partially overlap but they suggest the existence of a distinct and significantly older crust for the Canaã domain compared to that of Rio Maria. This conclusion should be verified by additional geological and geochronological studies in other areas of the 'Transition' sub-domain. Nevertheless, it is likely that the Mesoarchean crust of Canaã had initiated its tectonic stabilization before that of Rio Maria and it is demonstrated that the entire Carajás domain was submitted to intense crustal reworking during the Neoproterozoic, whereas the Rio Maria domain was stabilized at the end of the Mesoarchean.

7.4. A brief comparison with other Archean cratons

Archean cratons are commonly composed of three main lithologic units: (1) a gneissic basement of tonalitic-trondhjemitic-granodioritic (TTG) composition; (2) greenstone belts; (3) K-rich granites, generated generally late in the geological evolution of the craton (Moyen et al., 2003). This general picture is quite similar to that registered in the Rio

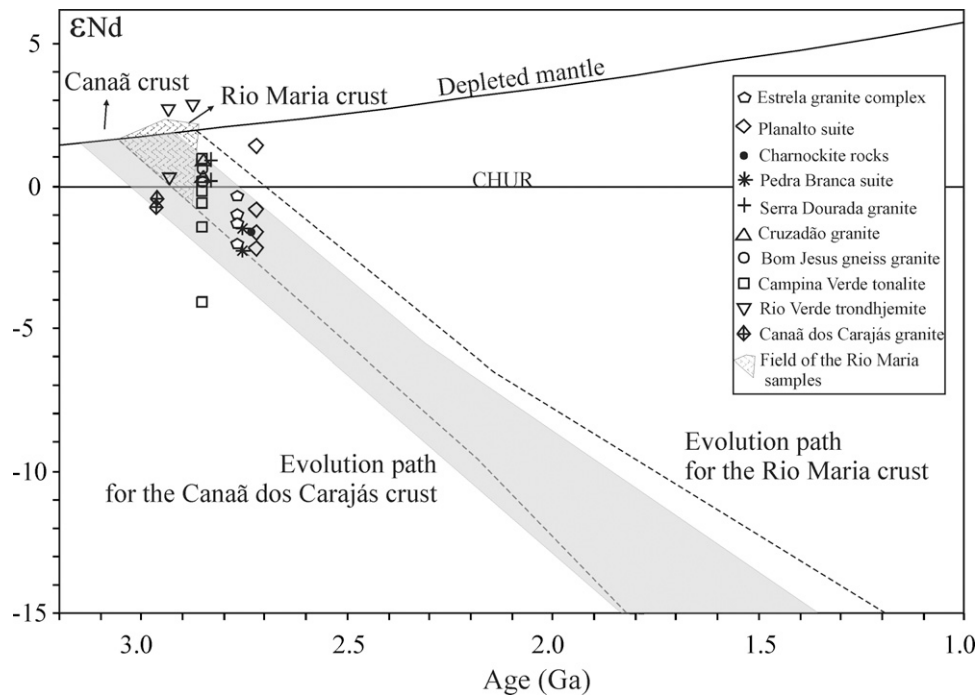


Fig. 13. ϵ Nd vs. age diagram for the Archean granitoids of the Canaã area of the Carajás province. The field of the Archean rocks of the Rio Maria domains and the evolution paths for the rocks of Rio Maria (Rämö et al., 2002) and Canaã (this work) are indicated. Data of the Estrela granite complex (Barros et al., 2009) are shown for comparison.

Maria domain but it differs substantially from that observed in the Canaã area of the Carajás province. In the following, a preliminary comparison between the evolution of the Carajás province and those of other Archean terranes is presented. We have selected the Dharwar and Karelian cratons, as well as the Limpopo belt for comparison.

The Dharwar craton (Jayananda et al., 2006; Jayananda and Chardon, 2011) is divided into two large domains, the western and eastern Dharwar craton, and has a longer evolution in time compared to the Carajás province. In the western Dharwar craton, the dominant rocks are TTG series (3.4–3.2 Ga, Peninsular gneisses) and supracrustal greenstone sequences (the 3.6–3.2 Ga, Sargur Group, and the 3.0–2.6 Ga, Dharwar Supergroup). Potassic plutons were formed during the Mesoarchean (ca. 3.0 Ga) and Neoproterozoic (ca. 2.6 Ga). In the eastern Dharwar craton, >3.0 Ga old basement relicts of TTG and 2.7–2.55 Ga greenstone belts were identified but the dominant rocks are the 2.56–2.51 Ga Neoproterozoic dominantly calc-alkaline to potassic granitoids, which include the classical Closepet granite (Moyen et al., 2003). The southern part of the craton was affected by granulitic metamorphism at the end of the Neoproterozoic (2.56–2.50 Ga). The evolution of the Dharwar craton extended over a large period of time (ca. 1.0 Ga) compared to the Carajás province (Fig. 12a). It is concluded that the tectonic and magmatic evolution of the Dharwar craton differs in its essence of that registered in the Carajás province.

The evolution of the Karelian province in Finland (Käpyaho et al., 2006; Heilimo et al., 2011) was concentrated in the Mesoarchean and Neoproterozoic (generally 2.95–2.50 Ga; Heilimo et al., 2011) and involved the rock types generally found in classical Archean terranes. The kind of magmatic rocks and their succession in time is quite similar to that described in the Rio Maria domain (Oliveira et al., 2009a, 2010a; Almeida et al., 2011); however the main geological units in Karelia were formed in between 2.83 and 2.68 Ga (Käpyaho et al., 2006), whereas the main period of new crust formation is a little older in Rio Maria (2.98–2.86 Ga). The contrasts between the Karelia province evolution and that of the Carajás province are even stronger in the case of the Carajás domain,

including the Canaã area. In this case, besides the difference in ages between both terranes, the main rocks formed during the Neoproterozoic are quite distinct in both provinces, suggesting contrasting tectonic evolution for them.

The Limpopo Belt is a polymetamorphic terrain situated between the Zimbabwe and Kaapvaal craton on southern Africa (Kröner et al., 1999). It was divided into three zones: a central zone bordered by two marginal zones that resulted of the crustal reworking of the adjacent Zimbabwe (to the North) and Kaapvaal cratons (to the South). This belt was interpreted as the result of a tectonic collision between the Kaapvaal and Zimbabwe cratons at ca. 2.70–2.65 Ga (Barton and Van Reenen, 1992; Rollinson, 1993). The two marginal zones should represent the equivalent lithologies of the adjacent cratons submitted to higher deformation and metamorphic grade (Kreissig et al., 2000). A high-grade metamorphism occurred at 2.7–2.5 Ga (Holzer et al., 1999) and its age is coincident with a main event of granitoid magmatism across the Limpopo belt. During this event pyroxene-bearing and pyroxene-free granitoids, as exemplified by the Matok pluton (Raposo, 2010), were generated. Despite the unequivocal contrasts, there are apparently some relevant similarities between the Limpopo belt and Carajás domain tectonic evolution. The most relevant aspect is that both provinces were strongly reworked during the Neoproterozoic and produced at that time an assemblage of pyroxene-bearing and pyroxene-free granitoids that are related to the generation of magmas in hot zones of the deep crust, possibly due to collisional tectonic processes. The analogies in evolution of the study area with hot magmatic zones, not only in the Archean but also during the Proterozoic (Smithies et al., 2011), should be deeply investigated in the future to clarify the origin of the Neoproterozoic magmatism found in the Canaã area.

8. Conclusions

- (1) Systematic geological mapping, petrographic, geochemical, geochronological, and Nd isotope studies on Archean granitoids in the Canaã dos Carajás area of the Carajás province led to the discovery of new temporal and compositional groups of

Mesoarchean to Neoproterozoic granitoids in the Canaã area of the Carajás domain, adjacent to the Rio Maria domain.

- (2) The granitoids form four age groups: (1) The protolith of the mafic granulites and enderbites of the Pium complex, the Bacaba tonalite and other coeval rocks, as indicated by inherited zircons, were formed at 3.05–3.0 Ga; (2) both tonalitic-trondhjemitic and granitic suites were crystallized at 2.96–2.93 Ga (Rio Verde TTG and Canaã dos Carajás granites); (3) at 2.87–2.83 Ga were formed the Campina Verde tonalite, the Rio Verde trondhjemitic and the Serra Dourada granite. The Bom Jesus and Cruzado granites had a complex evolution and their minimum crystallization age is 2.83 Ga; and, (4) at 2.75–2.73 Ga, a tonalitic-trondhjemitic unit (Pedra Branca suite) and granitic (Planalto suite), as well as charnockitic rocks were formed.
- (3) Two compositional groups of granitoids were distinguished: (1) minor tonalitic-trondhjemitic units which are either geochemically different (Campina Verde and Pedra Branca) or similar to Archean TTGs (Rio Verde) and (2) major granitic units encompassing calc-alkaline (Canaã dos Carajás, Bom Jesus, and Serra Dourada), transitional (Cruzado) and alkaline (Planalto) granites. The granitic units cover more than 60% of the Canaã surface and are formed essentially by monzogranites and syenogranites.
- (4) The Canaã area differs from the Rio Maria and other granite-greenstone terranes by the scarcity of TTGs, dominance of granites and absence of sanukitoids. The evolution of the Canaã area started at 3.2 Ga and was different from that of the juvenile Rio Maria domain. Nd results of the Canaã granitoids indicate a contribution from older crust. Also, there are no equivalents for the Neoproterozoic magmatism in the Rio Maria domain. The Mesoarchean Canaã crust was strongly reworked during Neoproterozoic (2.75–2.70 Ga) and was probably the substratum of the Neoproterozoic Carajás basin.
- (5) The evolution of the Carajás domain differs significantly from that of the classical granite-greenstone terranes such as Dharwar and Karelian cratons. It approaches in some aspects the evolution of the Limpopo belt, a polymetamorphic terrain situated between the Zimbabwe and Kaapvaal craton on South Africa, because the Carajás domain and the Limpopo belt were both strongly reworked during the Neoproterozoic. At that time, possibly as a consequence of collisional tectonics, pyroxene-bearing and pyroxene-free magmas were formed in hot zones of the deep crust.

Acknowledgements

A.A.S. Leite, C.E.M. Barros, and D.C. Oliveira are acknowledged for support in field work and A.S. Sardinha, A.C.B. Gomes, and M.A. Oliveira for previous work in the studied area; M.A. Galarza Toro, P.A. Santos, J.A.C. Almeida, M. Matteini, and B. Lima, for their assistance on Pb-evaporation and U–Pb LA-MC-ICPMS analyses; C.N. Lamarão and I.M.O. Ramalho are thanked for their assistance in the cathodoluminescence imaging and the team of the Geochronological Laboratory of the Brasília University for Nd isotope analyses. O.T. Rämö discussed a preliminary set of our geochronological data. The reviews by J. Halla and M.M. Pimentel and the editorial handling of M. Jayananda were greatly appreciated. This research received financial support from CNPq (R. Dall'Agnol—Grants 0550739/2001-7, 476075/2003-3, 307469/2003-4, 484524/2007-0; PRONEX—Proc. 66.2103/1998-0; G.R.L. Feio—CNPq scholarship), and Federal University of Pará (UFPA). This paper is a contribution to the Brazilian Institute of Amazonia Geosciences (INCT program—CNPq/MCT/FAPESPA—Proc. 573733/2008-2) and to the project IGCP-SIDA 599.

Appendix A. Analytical procedures for whole-rock chemical analyses

The chemical analyses were performed by ICP-OES for major elements and ICP-MS for trace-elements, including the rare-earth elements, at the Acme Analytical Laboratories Ltd. in Canada.

Appendix B. Analytical methods of Geochronology

Zircon concentrates were extracted from ca. 10 kg rock samples using conventional gravimetric methods of heavy mineral separation and magnetic (Frantz isodynamic separator) techniques at the Geochronology Laboratory of the Federal University of Pará (Pará-Iso/UFPA). Final purification was achieved by hand selecting through a binocular microscope and the zircon grains of each sample were then photographed under reflected light. For U–Pb LA-MC-ICPMS analyses, the zircon grains of each sample were mounted in epoxy resin, polished, and their internal structures were examined by cathodoluminescence (CL) imaging technique in a scanning electron microscope LEO 1430 at the Scanning Electron Microscopy Laboratory of the Geosciences Institute of UFPA.

For the Pb-evaporation method (Kober, 1987), individual selected zircon grains were encapsulated in the Re-filament used for evaporation, which was placed directly in front of the ionization filament. The Pb is extracted by heating in three evaporation steps at temperatures of 1450 °C, 1500 °C, and 1550 °C and loaded on an ionization filament. The Pb intensities were measured by each peak stepping through the 206–207–208–206–207–204 mass sequence for five mass scans, defining one data block with eight $^{207}\text{Pb}/^{206}\text{Pb}$ ratios. The weighted $^{207}\text{Pb}/^{206}\text{Pb}$ mean for each block is corrected for common Pb using appropriate age values derived from the two-stage model of Stacey and Kramers (1975), and results with $^{204}\text{Pb}/^{206}\text{Pb}$ ratios higher than 0.0004 and those that scatter more than two standard deviations from the average age value were discarded. The calculated age for a single zircon grain and its error, according to Gaudette et al. (1998), is the weighted mean and standard error of the accepted blocks of data. The ages are presented with 2σ error.

The U–Pb LA-MC-ICPMS analyses were carried out using a New Wave UP213 Nd:YAG laser ($\lambda = 213$ nm), linked to a Thermo Finnigan Neptune multi-collector ICPMS at the Geochronology Laboratory of the University of Brasília. The analytical procedures were described by Buhn et al. (2009). The laser was run at a frequency of 10 Hz and energy of 0.4 mJ/pulse, ablation time of 40 s and a spot size of 30 μm in diameter. Plotting of U–Pb data was performed by ISOPLOT (Ludwig, 2001) and errors for isotopic ratios are presented at the 1σ level.

The analyses have been carried out using raster ablation method (Buhn et al., 2009) to prevent laser induced mass bias fractionation. The U–Pb raw data are translated to an Excel spreadsheet for data reduction and, when necessary, the laser induced mass bias was corrected using the method of Kosler et al. (2002). Common lead (^{204}Pb) interference and background correction, when necessary, were carried out by monitoring the ^{202}Hg and 204 mass ($^{204}\text{Hg} + ^{204}\text{Pb}$) during the analytical sessions and using a model Pb composition (Stacey and Kramers, 1975) when necessary. Reported errors are propagated by quadratic addition $[(2\text{SD}^2 + 2\text{SE}^2)^{1/2}]$ of external reproducibility and within-run precision. The external reproducibility is represented by the standard deviation (SD) obtained by repeated analyses ($n = 20$, $\sim 0.8\%$ for $^{207}\text{Pb}/^{206}\text{Pb}$ and $\sim 1\%$ for $^{206}\text{Pb}/^{238}\text{U}$) of standard zircon GJ-1, performed during analytical session, and the within-run precision is represented by the standard error (SE) that was calculated for each analysis.

For the exclusion of spot analyses on the calculation of U–Pb ages we have employed the general criteria adopted in the literature:

(1) the common lead content (the $^{206}\text{Pb}/^{204}\text{Pb}$ ratio should not be lower than 1000); (2) the degree of discordance (not using data where the discordance is higher than 10%); (3) the analytical precision (not using the data where the isotopic ratios have error greater than 3%). These general criteria were refined for each specific sample.

In the case of the samples dated by SHRIMP, sample GRD-47 was crushed, milled and sieved at 60 mesh and the heavy minerals were separated using heavy liquid (TBE tetra-bromo-ethane) and magnetic separation techniques. For the preparation of the samples ARC-109 and AMR-187B the techniques employed for zircon concentration were identical to those for Pb-evaporation and LA-MC-ICPMS methods. The final separation of the minerals was by hand picking the grains. These were mounted on epoxy discs (UWA 11-04 and UWA-06) with fragments of standards, ground and polished until nearly one-third of each grain was removed, and imaged (backscattered electrons) for their internal morphology using a scanning electron microscope at the Centre for Microscopy and Microanalysis at the University of Western Australia. The epoxy mounts were then cleaned and gold-coated to have a uniform electrical conductivity during the SHRIMP analyses.

The zircon standard used was BR266 zircon (559 Ma, 903 ppm U). The isotopic composition of zircon was determined using SHRIMP II (De Laeter and Kennedy, 1998), using methods based on those of Compston et al. (1992). A primary ion beam of ~ 3 nA, 10 kV O₂⁺ with a diameter of ~ 25 μm was focused onto the mineral. Each zircon U–Pb analysis on SHRIMP (Sensitive High-mass Resolution Ion MicroProbe) used five scans collecting nine measurements on each ($^{196}\text{Zr}^{20}$, ^{204}Pb , background, ^{206}Pb , ^{207}Pb , ^{208}Pb , ^{238}U , $^{248}\text{Th}^{0}$, and $^{254}\text{U}^{0}$). Corrections for common Pb were made using the measured ^{204}Pb and the Pb isotopic composition of Broken Hill galena. For each spot analysis, initial 60–90 s were used for pre-sputtering to remove the gold, avoiding the analysis of common Pb from the coatings. Zircons data are reduced using SQUID (Ludwig, 2002) software. Data were plotted on concordia diagrams using ISOPLOT/Ex software (Ludwig, 2001), in which error ellipses on Concordia plots are shown at the 95% confidence level (2σ). All ages given in text are weighted mean $^{207}\text{Pb}/^{206}\text{Pb}$ ages. Details of U–Pb data are presented in Table C.

Appendix C. Sm–Nd isotopic analyses

The analyses were performed at the Geochronology Laboratory of the University of Brasília and at the Isotope Geology Laboratory (Pará-Iso), of the UFPA Brazil, either using a Finnigan MAT 262 mass spectrometer.

Sm–Nd isotopic method of the Laboratory of the University of Brasília is described by Gioia and Pimentel (2000). Whole rock powders (ca. 50 mg) were mixed with ^{149}Sm – ^{150}Nd spike solution and dissolved in Savillex capsules. Sm and Nd extraction of whole rock samples followed conventional cation exchange techniques, using teflon columns containing LN-Spec resin (HDEHP–diethylhexyl phosphoric acid supported on PTFE powder). Sm and Nd samples were loaded on Re evaporation filaments of double filament assemblies and the isotopic measurements were carried out on a multi-collector Finnigan MAT 262 mass spectrometer in static mode. Uncertainties for Sm/Nd and $^{143}\text{Nd}/^{144}\text{Nd}$ ratios are better than $\pm 0.5\%$ (2σ) and $\pm 0.005\%$ (2σ), respectively, based on repeated analyses of international rock standards BHVO-1 and BCR-1.

For the Sm–Nd analyses obtained in the Isotope Geology Laboratory of the UFPA, was utilized the employed routine by Oliveira et al. (2009b) that consists of add ^{150}Nd – ^{149}Sm spike to the ca. 100 mg of rock and attack with HF + HNO₃ in Teflon vials inside PARR containers at 150 °C for one week. After evaporation, new additions of HF + HNO₃ are made, the solutions are dried, followed by dissolution with HCl (6N), drying, and finally dissolution

with HCl (2N). After the last evaporation, the REE are separated from other elements by cation exchange chromatography (Dowex 50WX-8 resin) using HCl (2N) and HNO₃ (3N). After that, Sm and Nd were separated from the other REE by anion exchange chromatography (Dowex AG1-X4 resin) using a mixture of HNO₃ (7N) and methanol. In both cases, the $^{143}\text{Nd}/^{144}\text{Nd}$ ratios were normalized to $^{146}\text{Nd}/^{144}\text{Nd}$ of 0.7219, and the decay constant used was 6.54×10^{-12} to $^{-1}$. The T_{DM} values were calculated using the model of De Paolo (1981).

Appendix D. Supplementary data

Supplementary data associated with this article can be found, in the online version, at <http://dx.doi.org/10.1016/j.precamres.2012.04.007>.

References

- Almeida, J.A.C., Dall'Agnol, R., Dias, S.B., Althoff, F.J., 2010. Origin of the Archean leucogranodiorite–granite suites: evidence from the Rio Maria terrane and implications for granite magmatism in the Archean. *Lithos* 120, 235–257.
- Almeida, J.A.C., Dall'Agnol, R., Oliveira, M.A., Macambira, M.J.B., Pimentel, M.M., Rämö, O.T., Guimarães, F.V., Leite, A.A.S., 2011. Zircon geochronology and geochemistry of the TTG suites of the Rio Maria granite–greenstone terrane: implications for the growth of the Archean crust of Carajás Province, Brazil. *Precambrian Research* 187, 201–221.
- Althoff, F.J., Barbey, P., Boullier, A.M., 2000. 2.8–3.0 Ga plutonism and deformation in the SE Amazonian craton: the Archean granitoids of Marajoara (Carajás Mineral province, Brazil). *Precambrian Research* 104, 187–206.
- Avelar, V.G., Lafon, J.M., Correia Jr., F.C., Macambira, E.M.B., 1999. O Magmatismo arqueano da região de Tucumã–Província Mineral de Carajás: novos resultados geocronológicos. *Revista Brasileira de Geociências* 29, 454–460.
- Barker, F., Arth, J.G., 1976. Generation of trondhjemite–tonalite liquids and Archean bimodal trondhjemite–basalt suites. *Geology* 4, 596–600.
- Barker, F., 1979. Trondhjemite: a definition, environment and hypotheses of origin. In: Barker, F. (Ed.), *Trondhjemites, Dacites and Related Rocks*. Elsevier, Amsterdam, pp. 1–12.
- Barros, C.E.M., Sardinha, A.S., Barbosa, J.P.O., Macambira, M.J.B., 2009. Structure, petrology, geochemistry and zircon U/Pb and Pb/Pb geochronology of the synkinematic Archean (2.7 Ga) A-type granites from the Carajás Metallogenic Province, northern Brazil. *Canadian Mineralogist* 47, 1423–1440.
- Barton Jr., J.M., Van Reenen, D.D., 1992. When was the Limpopo Orogeny? *Precambrian Research* 55, 7–16.
- Buhn, B., Pimentel, M.M., Matteini, M., Dantas, E.L., 2009. High spatial resolution analysis of Pb and U isotopes for geochronology by laser ablation multi-collector inductively coupled plasma mass spectrometry (LA-MC-ICP-MS). *Anais da Academia Brasileira de Ciências* 81, 1–16.
- Clemens, J.D., Yeaaron, L.M., Stevens, G., 2006. Barberton (South Africa) TTG magmas: geochemical and experimental constraints on source–rock petrology, pressure of formation and tectonic setting. *Precambrian Research* 151, 53–78.
- Compston, W., Williams, I.S., Kirschvink, J.L., Zichao, Z., Guogan, M., 1992. Zircon ages for the Early Cambrian timescale. *Journal of Geological Society London* 149, 171–184.
- Condie, K.C., 1993. Chemical composition and evolution of the upper continental crust: Contrasting results from surface samples and shale. *Chemical Geology* 104, 1–37.
- Condie, K.C., 2005. TTGs and adakites: are they both slab melts? *Lithos* 80, 33–44.
- Costa, J.B.S., Araújo, O.J.B., Santos, A., Jorge João, X.S., Macambira, M.J.B., Lafon, J.M., 1995. A Província Mineral de Carajás: aspectos tectono-estruturais, estratigráficos e geocronológicos. *Boletim do Museu Paraense Emílio Goeldi* 7, 199–235 (in Portuguese).
- Dall'Agnol, R., Teixeira, N.P., Rämö, O.T., Moura, C.A.V., Macambira, M.J.B., Oliveira, D.C., 2005. Petrogenesis of the Paleoproterozoic, rapakivi, A-type granites of the Archean Carajás Metallogenic Province, Brazil. *Lithos* 80, 01–129.
- Dall'Agnol, R., Oliveira, M.A., Almeida, J.A.C., Althoff, F.J., Leite, A.A.S., Oliveira, D.C., Barros, C.E.M., 2006. Archean and Paleoproterozoic granitoids of the Carajás Metallogenic Province, eastern Amazonian Craton. In: Dall'Agnol, R., Rosa-Costa, L.T., Klein, E.L. (Eds.), *Symposium on Magmatism, Crustal Evolution, and Metallogenesis of the Amazonian Craton*. Belém, PRONEX-UFPA-SBGNO, pp. 99–150 (Volume and Field Trip Guide).
- Davis, W.J., Fryer, B.J., King, J.E., 1994. Geochemistry and evolution of late Archean plutonism and its significance to the tectonic development of the Slave Craton. *Precambrian Research* 67, 207–241.
- Debon, F., Le Fort, P., 1988. A cationic classification of common plutonic rocks and their magmatic associations: principles, method, applications. *Bulletin on Mineralogy* 111, 493–510.
- De Laeter, J.R., Kennedy, A.K., 1998. A double focusing mass spectrometer for geochronology. *International Journal of Mass Spectrometry* 178, 43–50.
- De Paolo, D.J., 1981. Neodymium isotope in the Colorado Front Range and crust–mantle evolution in the Proterozoic. *Nature* 291, 193–196.

- Domingos, F.H., 2009. The Structural Setting of the Canaã dos Carajás Region and Sossego-Sequeirinho Deposits, Ph.D. Thesis. University of Durham, Carajás–Brazil, England, 483p.
- Feio, G.R.L., Dall'Agnol, R., Dantas, E.L., Macambira, M.B., Gomes, A.C.B., Sardinha, A.S., Santos, P.A., 2012. Geochemistry, geochronology, and origin of the Neoproterozoic Planalto Granite suite, Carajás, Amazonian craton: A-type or hydrated charnockitic granites. <http://dx.doi.org/10.1016/j.lithos.2012.02.020>.
- Feio, G.R.L., Dall'Agnol, R., submitted for publication. Geochemistry and Petrogenesis of the Mesoarchean Granites from the Canaã dos Carajás Area, Carajás Province, Brazil: Implications for the Origin of Archean. *Lithos*.
- Fossen, H., Tikoff, B., 1998. Extended models of transpression and transtension, and application to tectonic settings. In: Holdsworth, R.E., Strachan, R.A., Dewey, J.F. (Eds.), *Continental Transpression and Transtensional Tectonics*. Geological Society of London, pp. 15–33 (Special Publication 135).
- Frost, B.R., Barnes, C., Collins, W., Arculus, R., Ellis, D., Frost, C., 2001. A chemical classification for granitic rocks. *Journal of Petrology* 42, 2033–2048.
- Gabriel, E.O., Oliveira, D.C., Macambira, M.J.B., 2010. Caracterização geológica, petrográfica e geocronológica de ortopiroxênio-trondhjemitos (leucoenderbitos) da região de Vila Cedere III, Canaã dos Carajás-PA, Província Mineral de Carajás. In: SBG, Congresso Brasileiro de Geologia, 45, CDrom (in Portuguese).
- Gaudette, H.E., Lafon, J.M., Macambira, M.J.B., Moura, C.A.V., Scheller, T., 1998. Comparison of single filament Pb evaporation/ionization zircon ages with conventional U–Pb results: examples from the Precambrian of Brazil. *Journal of South American Earth Sciences* 11 (4), 351–363.
- Gibbs, A.K., Wirth, K.R., Hirata, W.K., Olszewski Jr., W.J., 1986. Age and composition of the Grão Pará Group volcanics. Serra dos Carajás. *Revista Brasileira de Geociências* 16, 201–211.
- Gioia, S.M.C.L., Pimentel, M.M., 2000. The Sm–Nd Isotopic Method in the Geochronology Laboratory of the University of Brasília. *Anais da Academia Brasileira de Ciências* 72, 219–246.
- Gomes, A.C.B., Dall'Agnol, R., 2007. Nova associação tonalítica-trondhjemítica Neoproterozoica na região de Canaã dos Carajás: TTG com altos conteúdos de Ti, Zr e Y. *Revista Brasileira de Geociências* 37, 182–193 (in Portuguese).
- Goodwin, A.M., 1991. *Precambrian Geology: The Dynamic Evolution of the Continental Crust*. Academic Press, London, 666 pp.
- Halla, J., 2005. Late Archean high-Mg granitoids (sanukitoids) in the Southern Karelian craton, Eastern Finland. *Lithos* 79, 161–178.
- Heilimo, E., Halla, J., Huhma, H., 2011. Single-grain zircon U–Pb age constraints of the western and eastern sanukitoid zones in the Finnish part of the Karelian Province. *Lithos* 121, 87–99.
- Holzer, L., Barton Jr., J.M., Paya, B.K., Kramers, J.D., 1999. Tectonothermal history in the western part of the Limpopo belt: test of the tectonic models and new perspectives. *Journal of African Earth Sciences* 28, 383–402.
- Huhn, S.B., Macambira, M.J.B., Dall'Agnol, R., 1999. Geologia e geocronologia Pb/Pb do granito alcalino arqueano Planalto, região da Serra do Rabo, Carajás-PA. *Simpósio de Geologia da Amazônia* 6, 463–466 (in Portuguese).
- Irvine, T.N., Baragar, W.R.A., 1971. A guide to the chemical classification of the common volcanic rocks. *Canadian Journal of Earth Sciences* 8, 523–547.
- Jayananda, M., Chardon, D., Peucat, J.J., Capdevila, R., 2006. 2.61 Ga potassic granites and crustal reworking in the western Dharwar craton, southern India: tectonic, geochronologic and geochemical constraints. *Precambrian Research* 150, 1–26.
- Jayananda, M., Chardon, D., 2011. Geology of the Dhawar Craton. In: Jayananda, M., Ahmad, T., Chardon, D. (Eds.), *International Symposium on Precambrian Accretionary Orogens and Field workshop in the Dharwar Craton, Southern India*. University of Delhi and Geological society of India, India, p. 51p.
- Käpyaho, A., Mänttari, I., Huhma, H., 2006. Growth of Archean crust in the Kuhmo district Eastern Finland: U–Pb and Sm–Nd isotope constraints on plutonic rocks. *Precambrian Research* 146, 95–119.
- Kober, B., 1987. Single-grain evaporation combined with Pb+ emitter bedding for $^{207}\text{Pb}/^{206}\text{Pb}$ age investigations using thermal ion mass spectrometry, and implications to zirconology. *Contributions to Mineralogy and Petrology* 96, 63–71.
- Kosler, J., Fonneland, H., Sylvester, P., Tubrett, M., Pedersen, R.B., 2002. U–Pb dating of detrital zircons for sediment provenance studies: a comparison of laser ablation ICPMS and SIMS techniques. *Chemical Geology* 182, 605–618.
- Kreissig, K., Nägler, T.F., Kramers, J.D., Van Reenen, D.D., Smit, C.A., 2000. An isotopic and geochemical study of the northern Kaapvaal Craton and the Southern Marginal Zone of the Limpopo Belt: are they juxtaposed terranes? *Lithos* 50, 1–25.
- Kröner, A., 1991. Tectonic evolution in the Archean and Proterozoic. *Tectonophysics* 87, 393–410.
- Kröner, A., Jaeckel, P., Brandl, G., Nemchin, A.A., Pidgeon, R.T., 1999. Single zircon ages for granitoid gneisses in the Central Zone of the Limpopo Belt, southern Africa and geodynamic significance. *Precambrian Research* 93, 299–337.
- Leite, A.A.S., Dall'Agnol, R., Althoff, F.J., 1999. Geoquímica e aspectos petrogenéticos do Granito Xinguara, Terreno Granito-Greenstone de Rio Maria–Cráton Amazônico. *Revista Brasileira de Geociências* 23 (3), 429–436 (in Portuguese).
- Leite, A.A.S., Dall'Agnol, R., Macambira, M.J.B., Althoff, F.J., 2004. Geologia e Geocronologia dos granitoides Arqueanos da região de Xinguara (PA) e suas implicações na evolução do Terreno Granito-Greenstone de Rio Maria. *Revista Brasileira de Geociências* 34, 447–458 (in Portuguese).
- Lobach-Zhuchenko, S.B., Rollinson, H.R., Chekulav, V.P., Arestova, N.A., Kovalenko, A.V., Ivanikov, V.V., Guseva, N.S., Sergeev, S.A., Matukov, D.I., Jarvis, K.E., 2005. The Archean sanukitoid series of the Baltic Shield: geological setting, geochemical characteristics and implications for their origin. *Lithos* 79, 107–128.
- Ludwig, K.R., 2001. User's Manual for Isoplot/Ex Version 2.49 A Geochronological Toolkit for Microsoft Excel. Berkeley Geochronological Center (Special Publication 1, pp. 1–55).
- Ludwig, K.R., 2002. Squid 1.02. A User's Manual. Berkeley Geochronological Center, Berkeley, California, USA (Special Publication 2, 21 pp).
- Macambira, M.J.B., Lafon, J.M., 1995. Geocronologia da Província Mineral de Carajás: Síntese dos dados e novos desafios. *Boletim do Museu Paraense Emílio Goeldi* 7, 263–287 (in Portuguese).
- Macambira, M.J.B., Lancelot, J., 1996. Time constraints for the formation of the Archean Rio Maria crust, southeastern Amazonian Craton, Brazil. *International Geology Review* 38, 1134–1142.
- Machado, N., Lindenmayer, Z.G., Krogh, T.E., Lindenmayer, D., 1991. U–Pb geochronology of Archean magmatism and basement reactivation in the Carajás area, Amazon shield, Brazil. *Precambrian Research* 49, 329–354.
- Martin, H., 1994. The Archean grey gneisses and the gneisses of continental crust. In: Condie, K.C. (Ed.), *Developments in Precambrian Geology*. *Archean Crustal Evolution*, vol. 11. Elsevier, Amsterdam, pp. 205–259.
- Moreto, C.P.N., Monteiro, L.V.S., Xavier, R.P., Amaral, W.S., Santos, T.J.S., Juliani, C., Souza Filho, C.R., 2011. Mesoarchean (3.0 and 2.86 Ga) host rocks of the iron oxide–Cu–Au Bacaba deposit, Carajás Mineral Province: U–Pb geochronology and metallogenetic implications. *Mineralium Deposita* 46, 789–811.
- Moyen, J.F., Martin, H., Jayananda, M., Auvray, B., 2003. Late Archean granites: a typology based on the Dharwar Craton (India). *Precambrian Research* 127, 103–123.
- Moyen, J.F., Stevens, G., 2006. Experimental constraints on TTG petrogenesis: implications for Archean geodynamics. In: Benn, K., Mareschal, J.C., Condie, K.C. (Eds.), *Archean Geodynamics and Environments*. AGU, pp. 149–178.
- Nakamura, N., 1974. Determination of REE, Ba, Fe, Mg, Na, and K in carbonaceous and ordinary chondrites. *Geochimica et Cosmochimica Acta* 38, 757–775.
- Nisbet, E.G., 1987. *The Young Earth: An Introduction to Archean Geology*. Boston, Allen and Unwin, 402 p.
- Nogueira, A.C.R., Truckenbrodt, W., Pinheiro, R.V.L., 1995. Formação Águas Claras, Pré-Cambriano da Serra dos Carajás: redescrção e redefinição litostratigráfica. *Boletim Museu Paraense Emílio Goeldi* 7, 177–277 (in Portuguese).
- O'Connor, J.T., 1965. A classification for quartz-rich igneous rocks based on feldspar ratios. *US Geological Survey Professional Papers* 525, 79–84.
- Oliveira, M.A., Dall'Agnol, R., Althoff, F.J., Leite, A.A.S., 2009a. Mesoarchean sanukitoid rocks of the Rio Maria Granite-Greenstone Terrane, Amazonian craton, Brazil. *Journal of South American Earth Sciences* 27, 146–160.
- Oliveira, E.M., Lafon, J.M., Gioia, S.M.C.L., Pimentel, M.M., 2009b. Datação Sm–Nd em rocha total e granada do metamorfismo granulítico da região de Tartarugal Grande, Amapá Central. *Revista Brasileira de Geologia* 38 (1), 114–127 (in Portuguese).
- Oliveira, M.A., Dall'Agnol, R., Scaillet, B., 2010a. Petrological constraints on crystallization conditions of Mesoarchean Sanukitoid Rocks, Southeastern Amazonian Craton, Brazil. *Journal of Petrology* 51, 2121–2148.
- Oliveira, D.C., Santos, P.J.L., Gabriel, E.O., Rodrigues, D.S., Faresin, A.C., Silva, M.L.T., Sousa, S.D., Santos, R.V., Silva, A.C., Souza, M.C., Santos, R.D., Macambira, M.J.B., 2010b. Aspectos geológicos e geocronológicos das rochas magmáticas e metamórficas da região entre os municípios de Água Azul do Norte e Canaã dos Carajás–Província Mineral de Carajás. In: SBG, Congresso Brasileiro de Geologia, 45, CDrom (in Portuguese).
- Peccherillo, A., Taylor, S.R., 1976. Geochemistry of Eocene calc-alkaline volcanic rocks from the Kastamonu area, Northern Turkey. *Contribution to Mineralogy and Petrology* 58, 63–81.
- Pidgeon, R.T., Macambira, M.J.B., Lafon, J.M., 2000. Th–U–Pb isotopic systems and internal structures of complex zircons from an enderbite from the Pium Complex, Carajás Province, Brazil: evidence for the ages of granulites facies metamorphism and the protolith of the enderbite. *Chemical Geology* 166, 159–171.
- Pinheiro, R.V.L., Holdsworth, R.E., 1997. Reactivation of Archean strike-slip fault systems, Amazon region, Brazil. *Journal of the Geological Society* 154, 99–103.
- Rämö, O.T., Dall'Agnol, R., Macambira, M.J.B., Leite, A.A.S., Oliveira, D.C., 2002. 1.88 Ga oxidized A-type granites of the Rio Maria region, eastern Amazonian craton, Brazil: positively anorogenic! *Journal of Geology* 110, 603–610.
- Rapopot, M., 2010. Petrogenesis of the Matok pluton, South Africa: Implications on the Heat Source that Induced Regional Metamorphism in the Southern Marginal Zone of the Limpopo Belt, Master Thesis. University of Stellenbosch, South Africa, 117p.
- Ricci, P.S.F., Carvalho, M.A., 2006. Rocks of the Pium–Area, Carajás Block, Brazil–A Deep seated High-T Gabbroic Pluton (Charnokitoid-Like) with Xenoliths of Enderbitic Gneisses Dated at 3002 Ma—The Basement Problem Revisited. In: VIII Simpósio de Geologia da Amazônia, CDrom (in Portuguese).
- Rollinson, H.R., 1993. A terrane interpretation of the Archean Limpopo Belt. *Geological Magazine* 130, 755–765.
- Santos, J.O.S., Hartmann, L.A., Gaudette, H.E., Groves, D.I., McNaughton, N.J., Fletcher, I.R., 2000. A new understanding of the provinces of the Amazon Craton based on integration of field mapping and U–Pb and Sm–Nd geochronology. *Gondwana Research* 3, 453–488.
- Santos, R.D., Oliveira, D.C., 2010. Geologia, petrografia e caracterização geoquímica das rochas máficas do Complexo Pium–Província mineral de Carajás. In: Congresso Brasileiro de Geologia, 45, CDrom (in Portuguese).
- Sardinha, A.S., Dall'Agnol, R., Gomes, A.C.B., Macambira, M.J.B., Galarza, M.A., 2004. Geocronologia Pb–Pb e U–Pb em zircão de granitoides arqueanos da região de Canaã dos Carajás, Província Mineral de Carajás. In: Congresso Brasileiro de Geologia, 42, CDrom (in Portuguese).

- Sardinha, A.S., Barros, C.E.M., Krymsky, R., 2006. Geology, Geochemistry, and U–Pb geochronology of the Archean (2.74 Ga) Serra do Rabo granite stocks, Carajás Province, northern Brazil. *Journal of South American Earth Sciences* 20, 327–339.
- Silva, M.L.T., Oliveira, D.C., Macambira, M.J.B., 2010. Geologia, petrografia e geocronologia do magmatismo de alto K da região de Vila Jussara, Água Azul do Norte—Província Mineral de Carajás. In: SBG, Congresso Brasileiro de Geologia, 45, CDrom (in Portuguese).
- Smithies, R.H., 2000. The Archean tonalite–trondhjemite–granodiorite (TTG) series is not an analogue of Cenozoic adakite. *Earth and Planetary Science Letters* 182, 115–125.
- Smithies, R.H., Champion, D.C., 2000. The Archean high-Mg diorite suite: links to tonalite–trondhjemite–granodiorite magmatism and implications for early Archean crustal growth. *Journal of Petrology* 41 (12), 1653–1671.
- Smithies, R.H., Howard, H.M., Evins, P.M., Kirkland, C.L., Kelsey, D.E., Hand, M., Wingate, M.T.D., Collins, A.S., Belousova, E., 2011. High-temperature granite magmatism, crust–mantle interaction and the Mesoproterozoic Intracontinental evolution of the Musgrave Province, Central Australia. *Journal of Petrology* 52, 931–958.
- Souza, M.C., Oliveira, D.C., Macambira, M.J.B., Galarza, M.A., 2010. Geologia, petrografia e geocronologia do granito de alto K da região de Velha Canadá, município de Água Azul do Norte—Província Mineral de Carajás. In: SBG, Congresso Brasileiro de Geologia, 45, CDrom (in Portuguese).
- Souza, Z.S., Potrel, A., Lafon, J.M., Althoff, F.J., Pimentel, M.M., Dall’Agnol, R., Oliveira, C.G., 2001. Nd, Pb and Sr isotopes in the Identidade Belt, an Archean greenstone belt of Rio Maria region (Carajás Province, Brazil): implications for the geodynamic evolution of the Amazonian Craton. *Precambrian Research* 109, 293–315.
- Stacey, J.S., Kramers, J.D., 1975. Approximation of terrestrial lead isotope evolution by a two stage model. *Earth and Planetary Science Letters* 26, 207–221.
- Stern, R.A., Hanson, G.N., 1991. Archean high-Mg granodiorites: a derivative of light rare earth enriched monzodiorite of mantle origin. *Journal of Petrology* 32, 201–238.
- Sylvester, P.J., 1989. Post-collisional alkaline granites. *Journal of Geology* 97, 261–280.
- Sylvester, P.J., 1994. Archean granite plutons. In: *Condie, K. (Ed.), Archean Crustal Evolution*. Elsevier, Amsterdam, pp. 261–314.
- Tallarico, F.H.B., Figueiredo, B.R., Groves, D.I., Kositcin, N., McNaughton, N.J., Fletcher, I.R., Rego, J.L., 2005. Geology and Shrimp U–Pb geochronology of the Igarapé Bahia deposit, Carajás Copper–Gold belt, Brazil: an Archean (2.57 Ga) example of iron-oxide Cu–Au–(U-REE) mineralization. *Economic Geology* 100, 7–28.
- Tassinari, C.C.G., Macambira, M., 2004. A evolução tectônica do Craton Amazônico. In: Mantesso-Neto, V., Bartorelli, A., Carneiro, C.D.R., Brito Neves, B.B. (Eds.), *Geologia do Continente Sul Americano: Evolução da obra de Fernando Flávio Marques Almeida*. São Paulo, pp. 471–486 (in Portuguese).
- Teixeira, J.B.G., Eggler, D.H., 1994. Petrology, geochemistry, and tectonic setting of Archean basaltic and dioritic rocks from the N4 iron deposit, Serra dos Carajás, Pará, Brazil. *Acta Geologica Leopoldensia* 17, 71–114.
- Trendall, A.F., Basei, M.A.S., Laeter, J.R., Nelson, D.R., 1998. SHRIMP zircon U–Pb constraints on the age of the Carajás formation, Grão Pará group, Amazon Craton. *Journal of South American Earth Sciences* 11, 265–277.
- Vasquez, L.V., Rosa-Costa, L.R., Silva, C.G., Ricci, P.F., Barbosa, J.O., Klein, E.L., Lopes, E.S., Macambira, E.B., Chaves, C.L., Carvalho, J.M., Oliveira, J.G., Anjos, G.C., Silva, H.R., 2008. Geologia e Recursos Minerais do Estado do Pará: Sistema de Informações Geográficas–SIG: texto explicativo dos mapas Geológico e Tectônico e de Recursos Minerais do Estado do Pará, 328p (in Portuguese).